Trinity University
Digital Commons @ Trinity

Geosciences Faculty Research | Geosciences Department

3-10-2012

Cenozoic Tectonic Evolution of the Central Wassuk Range, Western Nevada, USA

Benjamin E. Surpless
Trinity University, bsurples@trinity.edu

Follow this and additional works at: https://digitalcommons.trinity.edu/geo_faculty

 Part of the Earth Sciences Commons

Repository Citation

Surpless, B. E. (2012). Cenozoic tectonic evolution of the central Wassuk Range, western Nevada, USA. *International Geology Review, 54*(5), 547-571. doi: 10.1080/00206814.2010.548117

This Article is brought to you for free and open access by the Geosciences Department at Digital Commons @ Trinity. It has been accepted for inclusion in Geosciences Faculty Research by an authorized administrator of Digital Commons @ Trinity. For more information, please contact jcostanz@trinity.edu.

International Geology Review
2011, iFirst article, 1–25

Taylor & Francis
Taylor & Francis Group

Cenozoic tectonic evolution of the central Wassuk Range, western Nevada, USA

Benjamin E. Surpless*

Department of Geosciences, Trinity University, One Trinity Place, San Antonio, TX 78212, USA

(*Accepted 12 December 2010*)

The central Wassuk Range is ideally located to investigate the interplay of Basin and Range extension and Walker Lane dextral deformation along the western Nevada margin of the Basin and Range province. To elucidate the Cenozoic evolution of the range, the author conducted geologic mapping, structural data collection and analysis, geochemical analysis of igneous lithologies, and geochronology. This research delineates a three-stage deformational history for the range. A pulse of ENE–WSW-directed extension at high strain rates (~8.7 mm/yr) was initiated immediately after the eruption of ~15 Ma andesite flows; strain was accommodated by high-angle, closely spaced (1–2 km), east-dipping normal faults which rotated and remained active to low angles as extension continued. A post-12 Ma period of extension at low strain rates produced a second generation of normal faults and two prominent dextral strike–slip faults which strike NW, subparallel to the dextral faults of the Walker Lane at this latitude. A new pulse of ongoing extension began at ~4 Ma and has been accomodated primarily by the east-dipping range-bounding normal fault system. The increase in the rate of fault displacement has resulted in impressive topographic relief on the east flank of the range, and kinematic indicators support a shift in extension direction from ENE–WSW during the highest rates of Miocene extension to WNW–ESE today. The total extension accommodated across the central Wassuk Range since the middle Miocene is >200%, with only a brief period of dextral fault activity during the late Miocene. Data presented here suggest a local geologic evolution intimately connected to regional tectonics, from intra-arc extension in the middle Miocene, to late Miocene dextral deformation associated with the northward growth of the San Andreas Fault, to a Pliocene pulse of extension and magmatism likely influenced by both the northward passage of the Mendocino triple junction and possible delamination of the southern Sierra Nevada crustal root.

Keywords: Wassuk Range; Basin and Range; Walker Lane; extension; dextral faults; volcanism; Mendocino triple junction; Sierra Nevada

Downloaded By: [Surpless, Benjamin E.] At: 14:16 19 April 2011

Introduction

Modern geodetic data (e.g. Minster and Jordan 1987; Dixon *et al.* 1995; Bennett *et al.* 1999; Kreemer *et al.* 2009) and historical seismicity (e.g. Eaton 1982; Eddington *et al.* 1987; Seedorff 1991; Wernicke 1992) suggest that the margins of the Basin and Range are among the most tectonically active regions in North America. Throughout Cenozoic and Quaternary time, the structural evolution of the western margin of the province has been complicated by the interplay of strike–slip deformation associated with the Walker Lane (Figure 1), which accommodates up to 25% of the relative motion between the Pacific and North American plates (e.g. Minster and Jordan 1987; Bennett *et al.* 1999), and normal faulting related to Basin and Range extension. These competing tectonic influences have resulted in significant regional variation in the style and magnitude of deformation along the western margin of the province (e.g. Gilbert and Reynolds 1973; Proffett 1977; Dilles and Gans 1995; Sawyer and Briggs 2001; Stockli *et al.* 2002, 2003; Armstrong *et al.* 2003; Lerch *et al.* 2004; Colgan *et al.* 2006).

At ~39°N, deformation associated with Walker Lane dextral motion has been focused east of Walker Lake, where the strike–slip faults of the Gillis and Gabbs Valley ranges became active as early as 24 Ma (Figure 2; e.g. Ekren *et al.* 1980; Ekren and Byers 1984; John 1992) and have accommodated as much as 80 km of dextral displacement since 15–10 Ma (e.g. Hardyman and Oldow 1991; Oldow *et al.* 1994); an acceleration of slip commenced at about 10 Ma (Hardyman and Oldow 1991) to 7 Ma (Dilles and Gans 1995). West of Walker Lake, N–S-trending ranges and intervening basins are primarily the result of westward tilting of fault blocks along major east-dipping normal faults since 15 Ma (Figure 2; e.g. Proffett 1977; Dilles and Gans 1995; Schweickert *et al.* 2000; Stockli *et al.* 2002; Surpless *et al.* 2002). Thus, the Wassuk Range is the approximate boundary between active dextral motion associated with the Walker Lane and Basin and Range extension (e.g. Oldow *et al.* 1994, 2003; Wesnousky 2005; Surpless 2008).

In the central Wassuk Range, fault blocks consist mostly of Jurassic and Cretaceous granitoids and country

*Email: bsurples@trinity.edu

ISSN: 0020-6814 print/1938-2839 online
© 2011 Taylor & Francis
DOI: 10.1080/00206814.2010.548117
http://www.informaworld.com

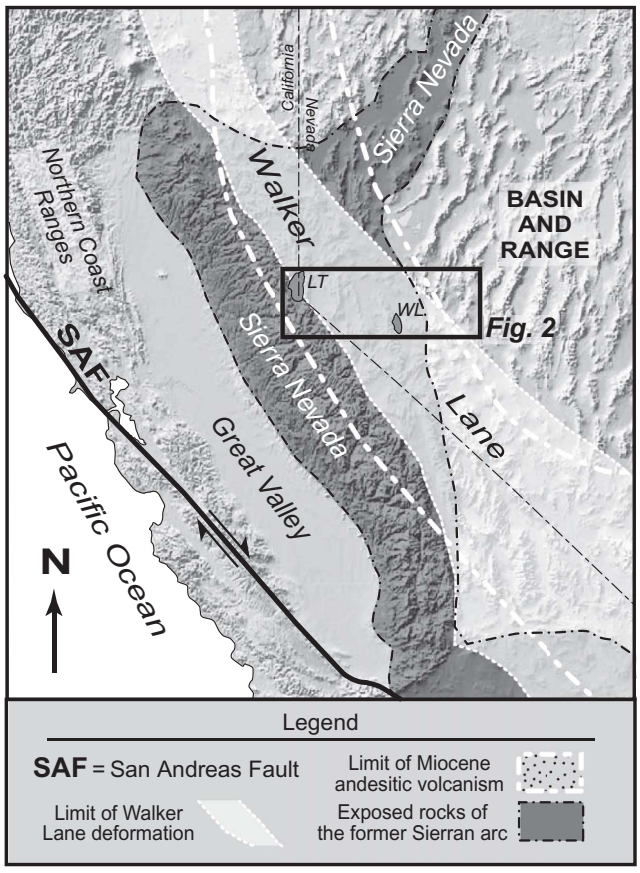

Figure 1. Shaded digital relief map of important geologic features of the western Basin and Range province. Features shown here include the approximate distribution of intrusive rocks of the former Sierran magmatic arc (modified from Burchfiel *et al.* 1992), the Walker Lane (white area; modified from Henry *et al.* 2007), the limit of Miocene andesitic volcanism (stippled region; modified from Lipman 1992), and the present-day San Andreas Fault system (SAF). The western boundary of the Walker Lane, as shown, is the approximate western boundary of Basin and Range deformation, as outlined by Cowan and Bruhn (1992). The white box is the area shown in Figure 2. LT, Lake Tahoe; WL, Walker Lake.

rock of the Sierran arc (Figure 1), unconformably overlain by Tertiary volcanic and sedimentary rocks. The ages and dips of Tertiary strata constrain the timing of fault motion, the magnitude of tilting associated with faulting, the axes of fault-block rotations, and the displacement along individual normal faults across the map area. The onset of significant extension is roughly coeval in the central Wassuk Range and the Yerington District of the Singatse Range (Figure 2), where the extrusion of voluminous Miocene andesitic lavas is closely linked to the onset of high rates of extension (Stockli *et al.* 2002). In addition to relating the onset of extension to magmatic events, the compositions of the magmas erupted prior to, during, and after the highest rates of extension can be related to the structural evolution of the area and more broadly to changes in regional tectonic conditions.

This study presents new geologic mapping, geochronology, geochemical, and structural data which help constrain the Tertiary evolution of the central Wassuk Range. Combined with previous studies (e.g. Bingler 1978; McIntyre 1990; Dilles 1993; Stockli *et al.* 2002; Wesnousky 2005), this work clearly demonstrates a relationship between the nature of volcanism and the extensional history of the range and addresses its ongoing evolution in the context of Walker Lane deformation.

Previous work in the central Wassuk Range

Previous workers in the Wassuk Range (e.g. McIntyre 1990; Dilles 1993; Stockli *et al.* 2002) documented a style and timing of extensional deformation similar to that in the Singatse Range to the west (Proffett 1977; Stockli *et al.* 2002; Surpless *et al.* 2002). Based on low-temperature thermochronologic data, Stockli *et al.* (2002) documented rapid extension in the central Wassuk Range between ~15 Ma and ~12 Ma, with little evidence for any significant cooling related to footwall exhumation prior to that period. Similarly, rapid extension in the Singatse Range took place between approximately 15.0 Ma and 13.8 Ma (Dilles and Gans 1995) along closely spaced (1–2 km) normal faults with up to 4 km of offset on each fault (Proffett 1977; Proffett and Dilles 1984). Three generations of high-angle normal faulting resulted in >150% extension and block rotations of 60°–90° in the Singatse Range during this period. In the Singatse Range, extension has continued since 13.8 Ma at a much lower rate (Dilles and Gans 1995).

During this same period in the northern Wassuk Range (Figure 2), dextral strike–slip faults moved synchronously with oblique-slip normal faults to accommodate an average of 50° stratal rotation of fault blocks, with a dominant extension directed WNW–ESE to NW–SE (Dilles 1993). The strike–slip faults were largely accommodation structures between zones of oppositely dipping normal faults and exhibit little lateral displacement (Dilles 1993), although these faults were subparallel to the most prominent faults in the Walker Lane to the east (e.g. the Benton Springs Fault; Figure 2). Similar to the Singatse Range to the west (Figure 2), this period of tectonism ended by 14 Ma in the northern Wassuk Range (Dilles 1993).

McIntyre (1990) documented the initiation of several dextral and oblique-slip faults in the Reese River–Penrod Canyon area in the late Miocene, following the pulse of large-magnitude extension in the Signatse and Wassuk ranges. The high-angle Reese River fault (RRF in Figure 3), subparallel to the dominant strike–slip faults in the eastern Walker Lane at this latitude (Figure 2), accommodated up to 3350 m of right lateral displacement and pre-dates the younger Penrod Canyon and Cottonwood

Downloaded By: [Surpless, Benjamin E.] At: 14:16 19 April 2011

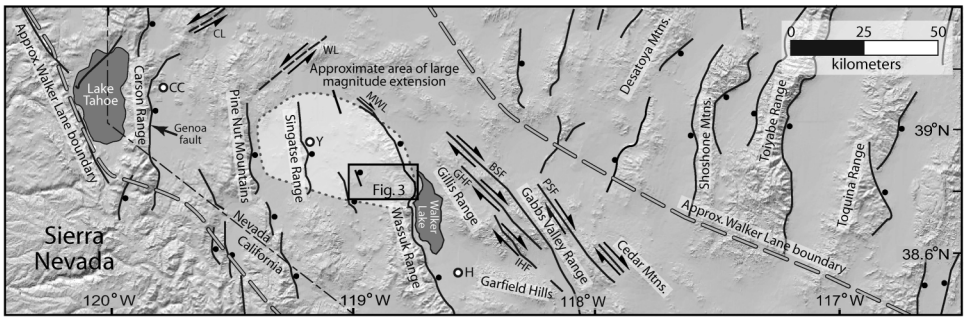

Figure 2. Digital topography and geographical features of the western margin of the Sierra Nevada–Basin and Range transition zone at ~39°N. Significant normal and dextral faults are indicated. The approximate locations of the Walker Lane boundaries are modified from Stewart (1993). The western boundary of the Walker Lane is also the approximate western limit of significant normal fault motion associated with Basin and Range extension. Dextral faults associated with the Walker Lane are to the east of Walker Lake. West of Walker Lake, normal faults with dip-slip motion dominate. The study area shown in Figure 3 is boxed, above. Significant middle Miocene extension affected the Singatse Range and the central and northern Wassuk Ranges, with no evidence for significant extension in either the Pine Nut Mountains or the ranges to the west of Walker Lake. BSF, Benton Spring Fault; CC, Carson City; CL, Carson lineament; GHF, Gumdrop Hills fault; H, Hawthorne; IHF, Indian Hills fault; MWL, modern Walker Lane (Dilles 1993); PSF, Petrified Springs fault; WL, Wabuska lineament; and Y, Yerington. Modified from Surpless (2008).

Downloaded By: [Surpless, Benjamin E.] At: 14:16 19 April 2011

Springs faults (McIntyre 1990). The Cottonwood Springs and Penrod Canyon faults (CSF and PCF, respectively, in Figure 3) moved synchronously and accommodated more than 4100 m of oblique-slip displacement in a geometry that created a pull-apart basin for the deposition and deformation of Miocene sediments with interbedded basalt flows (Figure 3; McIntyre 1990). This fault geometry and resulting deformation are consistent with significant oblique-dextral-slip along the range-front fault system of the Wassuk Range, but displacement along this cross-range fault system ended by 7 Ma, and there is no evidence for any new deformation associated with these faults since then (McIntyre 1990).

During the period of greatest activity along the Reese River–Penrod Canyon fault system, there is no evidence for any significant extensional deformation in the central Wassuk Range to the south (Stockli *et al.* 2002; Surpless *et al.* 2002). However, Stockli *et al*. (2002) suggest a renewed period of footwall cooling related to uplift along the present-day Wassuk Range normal fault system beginning at ~4 Ma and continuing to the present, based on (U–Th)/He and apatite fission-track data (location of samples shown in Figure 3). These thermochronologic data, along with the impressive topographic relief, well-defined fault-related triangular facets, and numerous fault-slip indicators along the east flank of the central Wassuk Range imply that extensional strain is now focused there, with no evidence for significant modern dextral deformation on most of the fault system (Demsey 1987; Zoback 1989; Wesnousky 2005; Bormann *et al.* 2010). However, near the northern terminus of the Wassuk Range, Dilles (1993) documented 1.3–2.8 km dextral offset accommodated by a splay of the range-front fault system (MWL in Figure 2). This fault displays evidence for oblique-dextral-normal slip and has likely been active during Quaternary time (Dilles 1993). If active during Quaternary time, this fault is the westernmost documented dextral deformation associated with the present-day Walker Lane. This fault is along strike of the most important dextral strike–slip faults of the central Walker Lane.

Pre-Cenozoic geology of the central Wassuk Range

The oldest units in the study area are metavolcanic rocks (Figures 3 and 4; map unit Trmv) which tentatively correlated with Triassic metavolcanic rocks in the Singatse Range (Bingler 1978). The plutonic rocks that intruded and metamorphosed these Triassic volcanic rocks were emplaced during Jurassic and Cretaceous Sierran arc magmatism related to subduction of the Farallon Plate beneath western North America (Figures 1 and 3; e.g. Burchfiel *et al.* 1992). The main phase of the Jurassic plutonic complex in the central Wassuk Range (Figures 3 and 4; map unit Jhqm) was originally named the Black Mountain pluton (Bingler 1978), but is here tentatively correlated with the intrusive episode that produced the Shamrock batholith, best described in the Singatse Range to the west (Figure 2) (Battles 1990, 1991). This correlation is based on similarities in petrographic, geochemical, and sodic and sodic-calcic alteration characteristics. In the central Wassuk Range, the Shamrock batholith consists of a main (most volumetrically significant) phase hornblende quartz monzonite (map unit Jhqm), and late phase rhyolite dikes and sills (map unit Jr) (Figures 3 and 4). In the central Wassuk Range, intense zones of channelized sodic and sodic-calcic alteration in the Buck Brush Spring block are bleached white in outcrop and occur as planar, 20°–30° east-dipping zones several metres thick.

Downloaded By: [Surpless, Benjamin E.] At: 14:16 19 April 2011

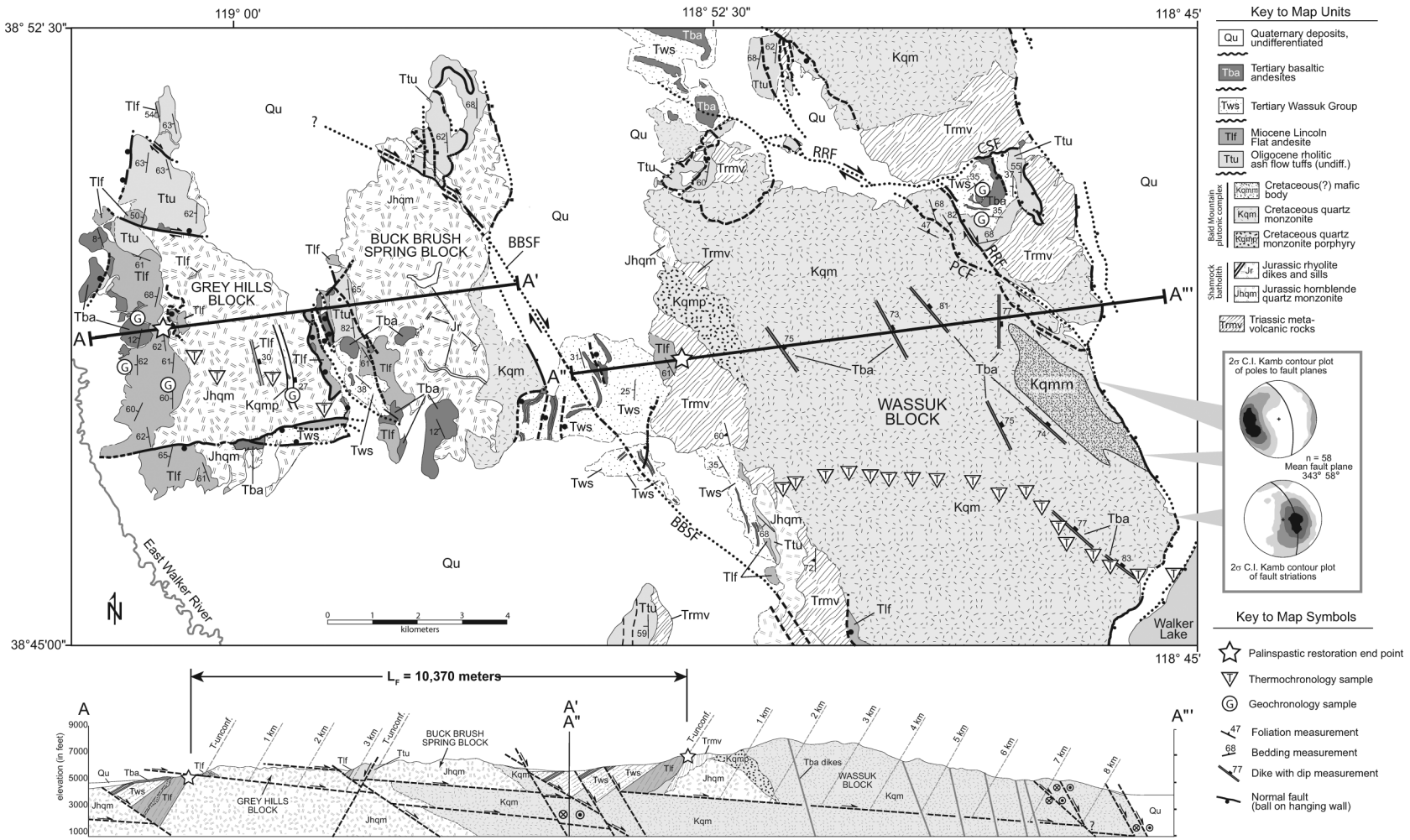

Figure 3. Simplified geologic map and cross-section of the central Wassuk Range, showing locations of thermochronology and geochronology samples. Distribution of map units based on Surpless (2010) as well as geologic mapping by Bingler (1978), at the 1:48,000 scale, and by McIntyre (1990), who focused on the Reese River, Penrod Canyon, and Cottonwood Springs fault systems (abbreviated RRF, PCF, and CSF, respectively). The Mickey Pass and Singatse silicic ash-flow tuffs are not differentiated here and are represented by map unit Ttu (Tertiary tuffs, undifferentiated). Dashed lines shown in cross-section indicate estimated pre-extensional palaeodepth below the Tertiary unconformity. The length used for calculations of cumulative extension is the distance between the Tlf/Jhqm contact on the west and the Tlf/Trmv contact on the east. The final length, post-extension (L_f), is 10,370 m. Fault plane and striation measurements of the Wassuk RBF on the east flank of the Wassuk block are shown on the right. Schematic stratigraphic section for important Mesozoic and Tertiary units is shown in Figure 4. Modified from Stockli *et al.* (2002) and Surpless (2010).

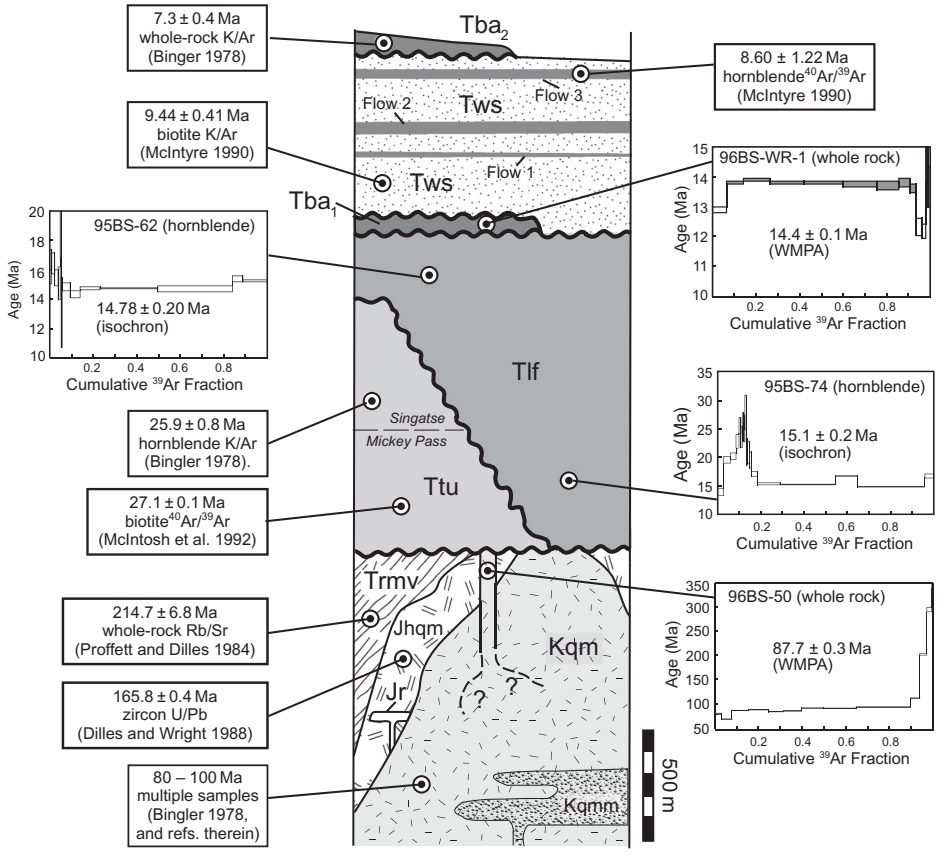

Figure 4. Schematic stratigraphic section of important Mesozoic and Tertiary map units in the central Wassuk Range, showing compilation of ages from the literature and those obtained in this study. Map unit Ttu consists of both the Mickey Pass and Singatse silicic ash-flow tuffs. See text for discussion of true unit thicknesses. Abbreviations and patterns shown on the section above are the same as those shown in Figure 3. Locations of samples dated in this study are shown in Figure 3. Age release spectra display $\pm 1\sigma$ without error in J (irradiation parameter). For complete description of $^{40}Ar/^{39}Ar$ analytical procedures and age data, see Appendices 1 and 2, respectively.

The Cretaceous Bald Mountain plutonic complex (Figures 3 and 4) displays only minor evidence for hydrothermal alteration and is best described by Bingler (1978). The complex consists of a main phase of quartz monzonite (Kqm), a structurally deep, xenolith- and mafic-enclave-rich phase (Kqmm), and a porphyritic, structurally shallow roof phase, a porphyritic quartz monzonite (Kqmp). A Kqmp dike crosscuts the Jurassic hornblende quartz monzonite (Jhqm) in the Grey Hills block and dips at 27° to the east, and a late-stage fine-grained quartz monzonite (Kqm) dike intrudes the Cretaceous complex and displays an eastward dip of 25°–30°. New geochronologic analysis of this dike yielded a whole-rock $^{40}Ar/^{39}Ar$ weighted mean plateau age (WMPA) of 87.7 ± 0.3 Ma (Figure 4), suggesting that most of the Cretaceous plutonic complex was emplaced by that time.

New trace-element data from the main phases of both the Jurassic and Cretaceous plutonic complexes show that they are enriched in Rb, Ba, Th, U, and K, and depleted in Ta, Zr, and Sm, relative to ocean island basalts (Figure 5A). These characteristics are consistent with crustal contamination at a plate margin that would be expected in subduction-related plutonic rocks (Figure 1). The range in elemental compositions for Jurassic and Cretaceous plutonic samples is displayed on other spidergrams for comparison (Figure 5).

Until the emplacement of volcanic rocks in the Oligocene (Figure 4), no further magmatism affected the central Wassuk Range. This local cessation in magmatism has also been documented throughout the western North American Cordillera and was likely caused by a change in the dip angle of the subducting Farallon Plate, resulting in cessation of Sierran arc magmatism (e.g. Severinghaus and Atwater 1990).

The Tertiary unconformity which cuts these older units (Figure 3) developed during Late Cretaceous–early Tertiary uplift and erosion, possibly the result of some combination of crustal thickening during Sierran magmatism and the Sevier orogeny (e.g. Wernicke 1992). The magnitude of uplift and erosion in the central Wassuk Range is poorly

Downloaded By: [Surpless, Benjamin E.] At: 14:16 19 April 2011

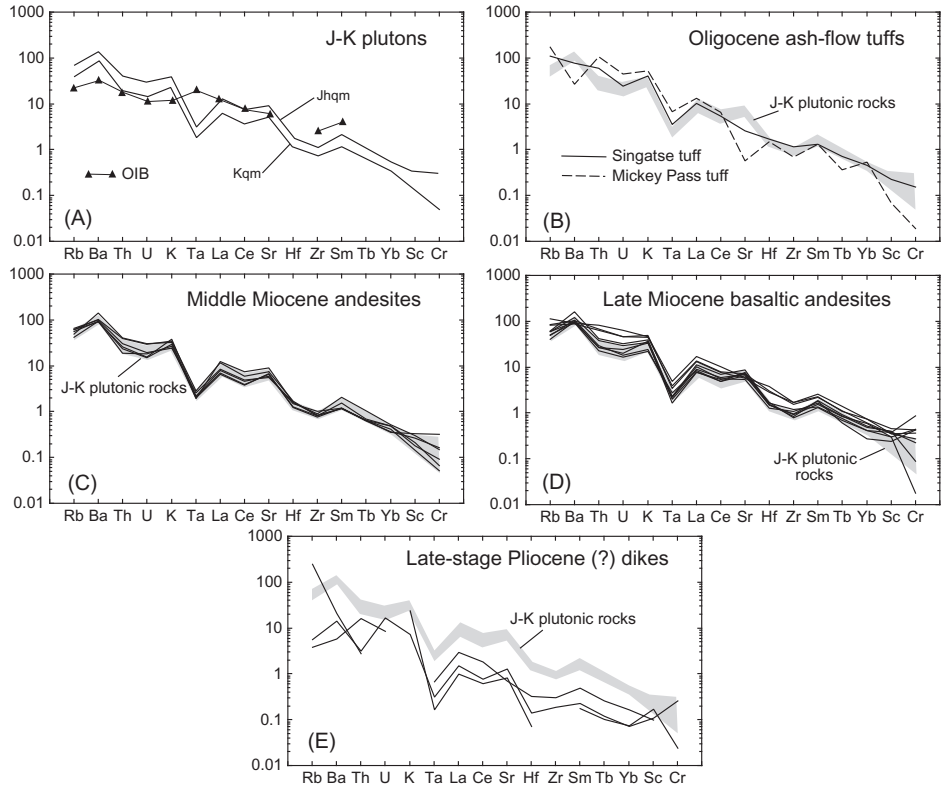

Figure 5. MORB-normalized trace-element spidergrams for Mesozoic plutons and Cenozoic volcanic rocks (normalization factors from Sun 1980; Saunders and Tarney 1984; Yb from Pearce 1983; Sc and Cr from Pearce 1982). (A) Representative samples from the main phases of Jurassic and Cretaceous plutonic complexes; (B) representative samples of Oligocene rhyolitic ash-flow tuffs compared to Jurassic and Cretaceous pluton data; (C) samples of middle Miocene andesite flows compared to Jurassic and Cretaceous pluton data; (D) late Miocene basaltic andesite samples compared to Jurassic and Cretaceous pluton data; and (E) late-stage Pliocene (?) dikes compared to Jurassic and Cretaceous pluton data. The compositional range of Jurassic and Cretaceous sample data is shaded grey in other spidergrams, for reference. Trace-element data are in Appendix 3.

Downloaded By: [Surpless, Benjamin E.] At: 14:16 19 April 2011

constrained by exposed geology, as no Mesozoic volcanic cover remains, but apatite fission-track-length modelling suggests a protracted period of post-Cretaceous uplift and denudation which continued until the eruption of silicic ash-flow tuffs in the Oligocene (Stockli *et al.* 2002). In the nearby Singatse Range (Figure 2), 2–4 km uplift and erosion occurred sometime between about 165 Ma and 30 Ma (e.g. Proffett and Dilles 1984; John *et al.* 1994), so it is likely that the exposures of Jurassic and Cretaceous plutonic units structurally below the Tertiary unconformity represent a minimum of 2 km pre-extensional emplacement depth in the central Wassuk Range (Figure 3).

Cenozoic volcanic and sedimentary rocks of the central Wassuk Range

Volcanic rocks exposed in the central Wassuk Range provide evidence for the episodic nature of magmatism throughout the Tertiary. The ages and geochemistry of these eruptive products can be related to tectonic conditions and can therefore help elucidate the interactions between magmatism and extension. In addition, Cenozoic volcanic and sedimentary units, including Oligocene rhyolite ash-flow tuffs, middle Miocene andesite and basaltic andesite flows, the well-bedded Wassuk Group, and late Miocene basaltic andesite flows aid in reconstruction of extensional deformation in the central Wassuk Range. The ages, unit thicknesses, and distributions of important volcanic rocks in the study area are listed in Table 1.

Oligocene rhyolitic ash-flow tuffs

The Mickey Pass and Singatse rhyolite ash-flow tuffs are best exposed in the northern Grey Hills and Buck Brush Springs fault blocks (map unit Ttu). The maximum combined stratigraphic thickness of these two tuffs, exposed on the northern part of the Grey Hills block, is approximately 1800 m (Table 1). It is likely that both the Mickey Pass and Singatse ash-flow tuffs originated from sources of the central Nevada caldera belt, flowing as far as 210 km (estimated pre-extension distance) from the east (Garside *et al.* 2002; Henry *et al.* 2009). Both ash-flow tuffs crop out as moderately resistant hills aligned parallel to the strike of

Table 1. Volcanism in the central Wassuk Range.

Age[a](Ma)	Map unit	Eruptive product(s)	Unit thickness	Distribution
26–27	Ttu	Rhyolitic ash-flow tuffs	1.8 km max.	Regional
~15	Tlf	Andesite lava flows	1.4 km max.	Regional
14.4	Tba_1	Basaltic andesite flow	<10 m	Local
9.4	Tws	Biotite-bearing air-fall tuff[b]	<1 m	Unknown
8.6	Tws	Basaltic andesite flow[b]	0 – 75 m	Local
7.3	Tba_2	Basaltic andesite flows	Variable	Unknown
Post-7.3 Ma[c]	–	Basaltic dikes	–	Unknown

Notes: [a]in central Wassuk Range
[b]interbedded with Wassuk Group sediments
[c]based on field relationships; see text for discussion and sources.

Downloaded By: [Surpless, Benjamin E.] At: 14:16 19 April 2011

compaction foliations, and the westward dip of these compaction foliations ranges from approximately 60° to 70° in the study area.

The Mickey Pass ash-flow tuff is a crystal-rich, multiple ash-flow tuff unit ranging in composition from rhyodacite to rhyolite and is best described by Proffett and Proffett (1976). Field data from this study reveal a maximum exposed thickness of 1050 m in the study area, where the unit unconformably overlies Mesozoic basement rocks. In the study area, the Mickey Pass tuff consists of light pinkish-red to medium reddish-brown, pumiceous, largely devitrified, coarse-grained vitric-crystal tuff. The most prominent phenocyrsts in hand sample are sanidine, quartz, and plagioclase, which make up 20–30% of the rock. Compacted pumice lapilli are ubiquitous and one of the main identifying features. The Mickey Pass tuff has been dated in the Singatse Range at 27.1 ± 0.1 Ma by $^{40}Ar/^{39}Ar$ analysis of biotite (McIntosh *et al.* 1992) (Figure 4) and has been identified as far north as Virginia City, Nevada (Table 1) (Bingler 1978).

In the study area, the Singatse ash-flow tuff is a multiple ash-flow unit made up of a basal vitrophyre, a glassy and lithic-rich horizon several tens of metres thick, and a dense, devitrified, buff to reddish-brown coloured tuff that comprises most of the unit, nearly identical to Singatse ash-flow as described in the Singatse Range by Proffett and Proffett (1976). Field data reveal a maximum exposed thickness of approximately 880 m in the study area, where the ash-flow tuff conformably overlies the Mickey Pass tuff. The Singatse ash-flow tuff is a distinctive, coarse-grained, hornblende-biotite quartz latite crystal tuff best described by Proffett and Proffett (1976). Sanidine, plagioclase, quartz, biotite, and rarely hornblende are present as visible phenocrysts in hand sample. K/Ar analysis of hornblende by Bingler (1978) revealed an age of 25.9 ± 0.8 Ma for the Singatse tuff (Figure 4).

The Oligocene Mickey Pass and Singatse ash-flow tuff (map unit Ttu) samples from the study area display trace-element signatures similar to the main phases of both Jurassic and Cretaceous plutonic complexes (Figure 5B), but are slightly enriched in Rb, Th, U, K, and Ta relative to the earlier Mesozoic units. This enrichment of the most incompatible elements might indicate a greater crustal component but could also be caused by fractional crystallization prior to the eruption of these silicic ash-flow units.

Middle Miocene andesites

The Lincoln Flat andesite (Tlf) is best exposed on the western margin of the Grey Hills block and reaches a maximum stratigraphic thickness of nearly 1400 m at that location (Table 1). The Lincoln Flat andesite has also been documented in the Singatse Range to the west (Figure 2; e.g. Proffett 1977) and in the northern Wassuk Range (Dilles 1993). Lincoln Flat andesite flows (map unit Tlf) unconformably overlie either Oligocene ash-flow tuffs (map unit Ttu) or Mesozoic basement units (Figures 3 and 4). The lower contact of the Lincoln Flat andesite is commonly marked by a thin (<0.5 m thick) palaeosol or poorly exposed conglomerate (<1 m thick) containing clasts of Oligocene ash-flow tuffs and/or Mesozoic quartz monzonite and metavolcanic rocks. Both the palaeosol and conglomerate are best exposed at several locations at the base of Lincoln Flat andesite flows on the west margin of the Grey Hills fault block (Figure 3). At some localities, andesite flows appear to dip at angles 5°–10° more shallowly to the west than the underlying Oligocene ash-flow units (Ttu), but this relationship is not well established. Dikes and plugs of the Lincoln Flat andesite are well exposed within and adjacent to the Grey Hills and Buck Brush Spring blocks, and where the relationship is best exposed, on the west flank of the Grey Hills block (Figure 3), these dikes and plugs appear to be sources for the mapped andesite flows. In addition, andesitic flow breccias are common within the thick sequence of Lincoln Flat andesite flows exposed on the west flank of the Grey Hills block (Figure 3). Most andesite flows in the study area dip to the west 55°–60° (Figure 3).

Andesite flows display flow foliations defined by alignment of both elongate hornblende (4–7%) and tabular

plagioclase (5–10%) phenocrysts within a light grey, microcrystalline groundmass. Plagioclase phenocrysts are euhedral to subhedral, commonly display oscillatory zoning, and average 2–7 mm in length. Fresh hornblende phenocrysts are euhedral to subhedral and average 2–5 mm in length, but hornblende phenocrysts are commonly replaced by magnetite due to oxidation at the time of flow emplacement. New $^{40}Ar/^{39}Ar$ analyses of hornblende at the base and top of the thickest section of map unit Tlf yield ages of 15.1 ± 0.1 Ma and 14.7 ± 0.1 Ma, respectively (Table 1; Figure 4), which are in agreement with ages from a hornblende andesite breccia at the base of the unit in the northern Wassuk Range dated by $^{40}Ar/^{39}Ar$ at 14.95 ± 0.24 Ma (Figure 4; Dilles and Gans 1995).

New trace-element analyses of middle Miocene andesite samples reveal a relatively homogeneous geochemical signature (Figure 5C) that is nearly identical to the older Jurassic and Cretaceous plutonic units. As with the Mesozoic plutonic units in the area (Figure 5C), these data suggest that the parental magmas of these flows were produced in a subduction setting and were affected by crustal contamination prior to eruption.

Middle Miocene basaltic andesite

A single, thin (<10 m thick; Table 1), poorly exposed basaltic andesite flow dips at approximately 35° west on the western portion of the Grey Hills block (Figure 3). Although not laterally extensive, this flow (Tba_1 in Figure 4) is an important structural marker for palinspastic restoration and is petrographically and compositionally similar to the younger basaltic andesites described in detail below. New geochronologic analysis of this basaltic andesite yields a $^{40}Ar/^{39}Ar$ whole-rock age of 14.4 ± 0.1 Ma (Table 1; Figure 4).

Middle–late Miocene Wassuk Group

The dominantly alluvial and fluvial sedimentary and interbedded volcanic rocks of the Wassuk Group (Tws) are best exposed at two loci of deposition: on the western margin of the Wassuk fault block and to the north of the Reese River–Penrod Canyon fault systems (Figure 3). At these localities, the map unit lies in angular unconformity with older Cenozoic rocks (Ttu and Tlf) and/or Mesozoic basement (Figure 3). The Wassuk Group sedimentary rocks most commonly crop out as buff to tan coloured, poorly cemented clast-supported conglomerates and clay-rich sandstones, and the two thick (10–20 m) interbedded basaltic andesite flows (Flows 2 and 3 in Figure 4) crop out as dark grey to black, homogeneous, sparsely porphyritic flows without evidence for bake zones at the lower contact with underlying Wassuk Group sedimentary rocks (McIntyre 1990; this study).

In the study area, interbedded sediments and volcanic flows of the Wassuk Group display a range of dips, from 17°–43° to the west (McIntyre 1990; this study). However, there is no clear systematic change in dip value with stratigraphic position within the Wassuk Group (i.e. shallower dips upsection caused by tilting associated with normal fault displacement), likely because folding associated with syn- and post-depositional dextral and oblique faulting at both localities has complicated the relationship between bedding dip value and the evolution of faulting in the area (Figure 3).

Field data indicate that Wassuk Group deposition was initially controlled by an east-dipping set of N- to NW-striking normal faults initiated at high angles (60°–70°) that now dip moderately to the west (McIntyre 1990; this study). At the northern depocentre, to the north of the Wassuk block (Figure 3), the faults which controlled initial deposition of the Wassuk Group are offset by younger NW-striking right-lateral strike- and oblique-slip faults such as the Reese River fault, which likely affected later deposition and caused folding of Wassuk Group sedimentary and volcanic rocks (McIntyre 1990). Similarly, at the depocentre on the western margin of the Wassuk block, motion along the high-angle (>70°) dextral Buck Brush Spring fault appears to have created drag folds which affect the entire sedimentary and volcanic stratigraphy of the Wassuk Group, suggesting that at least some motion along the Buck Brush Spring fault post-dates significant Wassuk Group deposition (this study) (Figure 3).

Gilbert and Reynolds (1973) obtained K–Ar ages on air-fall tuffs within the Wassuk Group of up to 12.5 million years to the south and west of the study area, suggesting that the faults which controlled initial sedimentation might have been active in the map area at that time. However, the oldest dateable horizon, an interbedded air-fall tuff sampled from near the base of section at the northern depocentre (Flow 1 in Figure 4), yielded a K–Ar biotite age of 9.44 ± 0.41 million years (McIntyre 1990). $^{40}Ar/^{39}Ar$ analysis of hornblende from interbedded basaltic andesite Flow 3 yielded an age of 8.63 ± 1.22 million years (McIntyre 1990; Table 1; Figure 4). Based on these dates and the age of unconformably overlying late Miocene basaltic andesite flows, McIntyre (1990) suggests that most Wassuk Group sedimentation at the northern depocentre was limited to a relatively short period, between ~9.5 Ma and ~7 Ma. At the depocentre on the western margin of the Wassuk fault block, the similarity in both the total thickness of the Wassuk Group and the positions of Flows 2 and 3 within the unit's stratigraphy, relative to the northern depocentre, are strong evidence for placing the same temporal constraints on Wassuk Group deposition at that locality.

Downloaded By: [Surpless, Benjamin E.] At: 14:16 19 April 2011

Downloaded By: [Surpless, Benjamin E.] At: 14:16 19 April 2011

Late Miocene basaltic andesites

Basaltic andesite lava flows (Tba_2) are exposed at many localities throughout the study area, but are most common on the western flanks of fault blocks (Table 1; Figure 3). In several cases, these flows unconformably overlie both the Wassuk Group and the faults which controlled Wassuk Group deposition (Figures 3 and 4; Bingler 1978; McIntyre 1990; this study). At other localities, these flows unconformably overlie other Cenozoic or Mesozoic map units. A prominent, but localized, red bake zone is common where basaltic andesite flows overlie Tertiary sediments. In isolated cases, the interior of these flows displays weak columnar jointing. These flows crop out as dark grey, homogeneous, porphyritic lava flows, with plagioclase and clinopyroxene present as phenocrysts. In some flows, minor hornblende or minor iddinsitized olivine are also visible as phenocrysts in hand sample.

These flows dip 12° or less to the west (Figure 3), with most flows dipping at 8°–12° W throughout the Singatse Range and Wassuk Range (Dilles and Gans 1995). Dikes of the same composition intrude the Cretaceous plutonic complex in the Wassuk block (Table 1; Figure 4), and usually strike to the NNW, dipping steeply (75°–80°) to the ENE. Whole-rock K/Ar analysis of these basaltic andesite flows in the central Wassuk Range reveals an age of 7.3 ± 0.4 million years (Figure 4; Bingler 1978).

New trace-element data suggest these late Miocene flows are geochemically similar to both the only exposed middle Miocene basaltic andesite flow and the basaltic andesite flows interbedded in the Tertiary Wassuk Group. In addition, all basaltic andesite samples display trace-element signatures almost identical to both the Lincoln Flat andesite (Figure 5D) and earlier Jurassic and Cretaceous plutonic complexes.

Pliocene (?) or younger dikes

After the extrusion of basaltic andesite lava flows during the late Miocene, no younger extrusive volcanic products have been identified in the study area. However, the intrusion of subvertical basaltic dikes (not shown in Figure 3) with no existing extrusive equivalents suggests that magmatism continued after the eruption of late Miocene basaltic andesites. The probable Pliocene (?) or younger age is based on the assumption that these dikes were intruded as subvertical, tabular bodies, an orientation that these dikes still display, suggesting no significant tilting since their intrusion.

New geochemical analyses of late-stage Pliocene (?) basaltic dike samples display depleted trace-element signatures relative to Oligocene ash-flow tuff, andesite, and basaltic andesite samples in the central Wassuk Range (Figure 5E). Based on these data, late-stage dikes were less affected by crustal contamination and/or fractional crystallization than other volcanic rocks in the central Wassuk Range.

Pliocene and younger deposits

Pliocene and younger sedimentary deposits remain undated and mostly consist of alluvial fanglomerates, sandstones, and siltstones as well as fluvial and colluvial unconsolidated deposits that were deposited in modern fault-bounded basins. At this latitude, deposition in most basins of the Basin and Range occurs in half-grabens that are bound on their western sides by east-dipping normal faults (Figure 2). Young sedimentary deposits in the map area are extensively reworked by slope and fluvial processes. Based on gravity estimates, the Walker Lake basin may contain up to 4 km of sedimentary fill of unknown age, with a minimum of 2–2.5 km normal offset documented along the range-bounding fault system (Dilles 1993).

Synthesis of structural and geochemical data

Significant westward tilting of several major fault blocks in the central Wassuk Range has exposed large sections of the pre-extensional upper crust (Stockli *et al.* 2002; Figure 3) and permitted a detailed evaluation of faulting in the central Wassuk Range. Although multiple generations of normal faults are evident in cross-section, the relative amount of extension accommodated by each generation varies significantly. In addition, the activity of dextral strike–slip faults in the study area and geochemical data from igneous rocks provide additional information that better constrains the driving factors that controlled this deformation. The Cenozoic tectonic history of the central Wassuk Range can be divided into four periods:

- **30–15 Ma:** little to no extension; emplacement of voluminous rhyolitic ash-flow tuffs near the beginning of this period; voluminous andesitic magmatism at the end of this period
- **15–12 Ma:** rapid extension and footwall uplift; cessation of andesitic magmatism; episodic, volumetrically minor, basaltic andesite eruptions
- **12–4 Ma:** lower rates of extension; episodic basaltic andesite eruptions; initiation and termination of dextral displacement
- **4 Ma–present:** elevated rates of extension accommodated almost exclusively by the east-dipping, range-bounding fault system; intrusion of trace-element depleted basaltic dikes.

These temporal divisions and kinematics of fault motion are based on cross-cutting relations between map units, the

axes and magnitudes of stratal tilts, exposure of the Tertiary unconformity, sparse slickenside data, geochronology, low-temperature thermochronology (Stockli *et al.* 2002), and previous work done in the region (Figure 2) (e.g. Bingler 1978; Proffett and Dilles 1984; McIntyre 1990; Dilles 1993). The characteristics of fault zones in the study area and palinspastic restoration of extension are required to best reconstruct the Cenozoic structural and magmatic evolution of the area.

Fault zone characteristics

Nearly all fault zones in the central Wassuk Range display structures characteristic of brittle deformation and consist predominantly of unconsolidated breccia and fault gouge. In the study area, few faults were well exposed and have been identified primarily by discordant field relationships. Lithologies adjacent to and within fault zones commonly display bleaching and/or red coloration (oxidation) associated with recent groundwater flow along fault surfaces, brecciation, fault gouge, and rarely, slickensides and/or silicification of fault surfaces. Copper minerals, such as malachite and chrysocolla, may be present where faults cut Mesozoic rocks and Tertiary basaltic andesites. At deep structural levels (palaeodepths of ~5–8 km; Figure 3), the Cretaceous Bald Mountain plutonic complex is commonly sheared and/or foliated, with a thin mylonite zone recognized at one locality, suggesting that ductile deformation may have played a significant role at these palaeodepths.

Palinspastic restoration of extension

Normal faults in the area may display listric geometries at depth, as documented in the Yerington District (e.g. Proffett 1977; Proffett and Dilles 1984), but without well-constrained subsurface fault geometries, including the rate of change in fault dip with depth, structural reconstructions presented here assume faults to be planar in the upper crust. The relative homogeneity of exposed pre-extensional upper crust, mostly quartz monzonite of map units Jhqm and Kqm, makes it difficult to conclusively determine that the Grey Hills, Buck Brush Spring, and Wassuk blocks are structurally intact, but apatite fission-track and (U–Th)/He data are consistent with intact upper-crustal sections (Stockli *et al.* 2002).

Line of section (A′–A‴) is approximately perpendicular to the axis of westward fault block tilting as defined by the strike of Tertiary unconformities, volcanic rocks, and sedimentary strata (Figure 3). Thus, this line of section is ideally located to use as much structural data as possible across the Grey Hills, Buck Brush Spring, and the Wassuk blocks. The 2350 m offset in the line of section (Figure 3) was included to take dextral strike–slip motion along the Buck Brush Spring fault into account, so that reconstructions of the earlier structural evolution of the central Wassuk Range would be more accurate. The calculated magnitude of extension in the palinspastic restoration of this section is based on the true dips shown in cross-section A–A‴.

The length used for calculations of cumulative extension is the distance between the Tlf/Jhqm contact on the west and the Tlf/Trmv contact on the east (Figure 3). At present (0 Ma), L_f (final length) is approximately 10,370 m as measured parallel to line of section A–A‴ (Figure 3). The present-day orientation of the Tertiary unconformity indicates a total post-15 Ma west tilt of ~60° (Figure 3). At ~15 Ma, this reconstruction indicates a length, L_o (original length), of approximately 3290 m (Figure 6). It is assumed that most, if not all, extension between ~15 Ma and ~12 Ma was accommodated by the earliest faults, which are now subhorizontal (Figure 3). Based on this reconstruction, these faults were spaced 1–2 km apart and accommodated ~4 km of displacement each, strikingly similar to the spacing and displacements displayed in the Yerington District to the west (e.g. Proffett and Dilles 1984).

The total extension derived from the palinspastic restoration of cross-section A–A‴ is 7080 m (10,370 m – 3290 m = 7080 m) or more than 300% strain. An approximate strain rate of approximately 8.7 mm/year is derived for the initial pulse of extension, based on the difference between lengths at ~15 Ma and ~14.4 Ma (Surpless 1999). The documented cumulative magnitude of westward fault-block tilting from 15 Ma to the present is consistent with palaeomagnetic data from the Wassuk fault block, which indicate at least 60° westward fault-block tilting of Mesozoic granitic rocks about a NNW-trending horizontal axis since Cretaceous cooling (J. Oldow and J. Geissman, personal communication 1997).

The potential presence of unmapped faults in the Buck Brush Springs block, the unknown dip of fault surfaces, and the unknown nature of the interaction of different generations of faults at depth all introduce possible errors into palinspastic restoration. Because of this unquantifiable uncertainty, the total extension (>300%) cannot be tightly constrained and should be considered an estimate derived from available structural and thermochronologic data.

30–15 Ma time interval

Field evidence and palinspastic restoration of extension suggest that significant topography had been established prior to the eruption of Oligocene ash-flow tuffs. Based on structural restoration (Figure 7), the silicic ash-flow tuffs (map unit Ttu) were deposited in a roughly N-trending valley (at a high angle to the line of section) that was at least 600 m deep. Because the Oligocene rhyolitic ash-flow tuffs unconformably overlie Mesozoic metavolcanics and plutonic rocks with no significant basal conglomerate or other sedimentary rocks present above the Tertiary unconformity,

Downloaded By: [Surpless, Benjamin E.] At: 14:16 19 April 2011

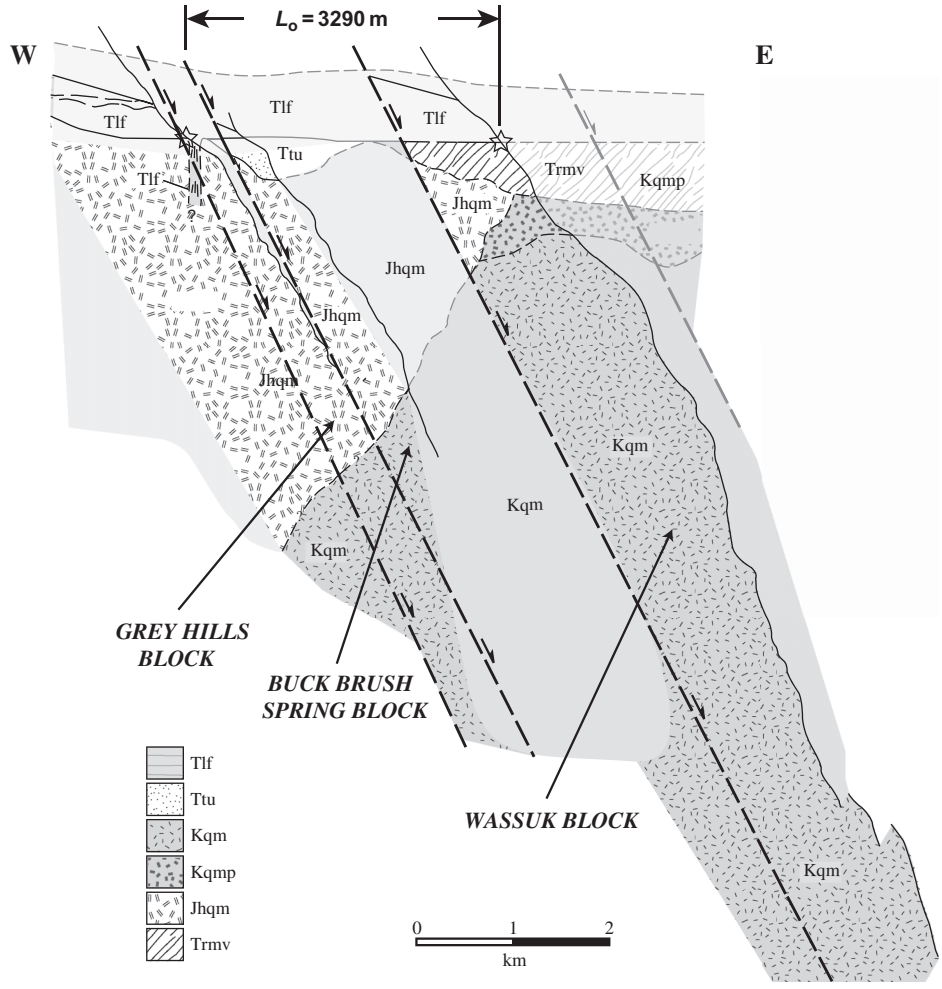

Figure 6. Pre-extensional (~15 Ma) palinspastic restoration of present-day geologic cross-section (Figure 3). Stars indicate the Tertiary unconformity exposed on the western margins of the Wassuk fault block and the Grey Hills fault block. The restored distance between these points (L_o) is 3290 m, relative to the present-day distance between those exposures (L_f) of 10,370 m (Figure 3), suggesting over 300% total extension across the central Wassuk Range. See text for discussion. Pre-extensional palaeodepths shown in Figure 3 are based on this reconstruction. Modified from Stockli *et al*. (2002).

Downloaded By: [Surpless, Benjamin E.] At: 14:16 19 April 2011

uplift and/or erosion probably were still the dominant processes in the central Wassuk Range when these Oligocene tuffs were erupted.

The regional distribution and relative homogeneity of the volcanic stratigraphy of these map units (e.g. Proffett and Proffett 1976; Dilles 1993; Dilles and Gans 1995; this study) suggests that these tuffs blanketed much of the region and were related to voluminous, explosive eruptions. These eruptions signalled a significant change in the tectonic setting of the central Wassuk Range. The timing of the eruption of these tuffs in the central Wassuk Range suggests that this volcanism was part of the initial southward sweep of intermediate to silicic volcanism from the Pacific Northwest (e.g. Stewart 1980; Glazner and Bartley 1984; Christiansen *et al.* 1992). This continental-scale event could be related to the hypothesized delamination of the Farallon slab from beneath North America, where the shallowly dipping Farallon slab either 'decomposed' due to conductive heating, detached, and fell away into the mantle, or re-steepened in dip, allowing deeper mantle to upwell beneath the continent beginning at about 60 Ma in the Pacific Northwest (e.g. Severinghaus and Atwater 1990). Although the eruption of these intermediate to silicic magmas has been closely tied to the onset of rapid extension at other localities (e.g. Gans *et al.* 1989, 2001), there is no field evidence for any significant extension related to this event in the central Wassuk Range.

Geochemical analyses of these rocks (Figure 5B) indicate that the generation and evolution of the source magmas involved a significant crustal component, permitting the inference that these magmas did not have an easy path to the surface. Instead, it is likely that the stress field at the time of eruption did not promote dilatational opening of pathways for the easy movement of magma upward or for

Downloaded By: [Surpless, Benjamin E.] At: 14:16 19 April 2011

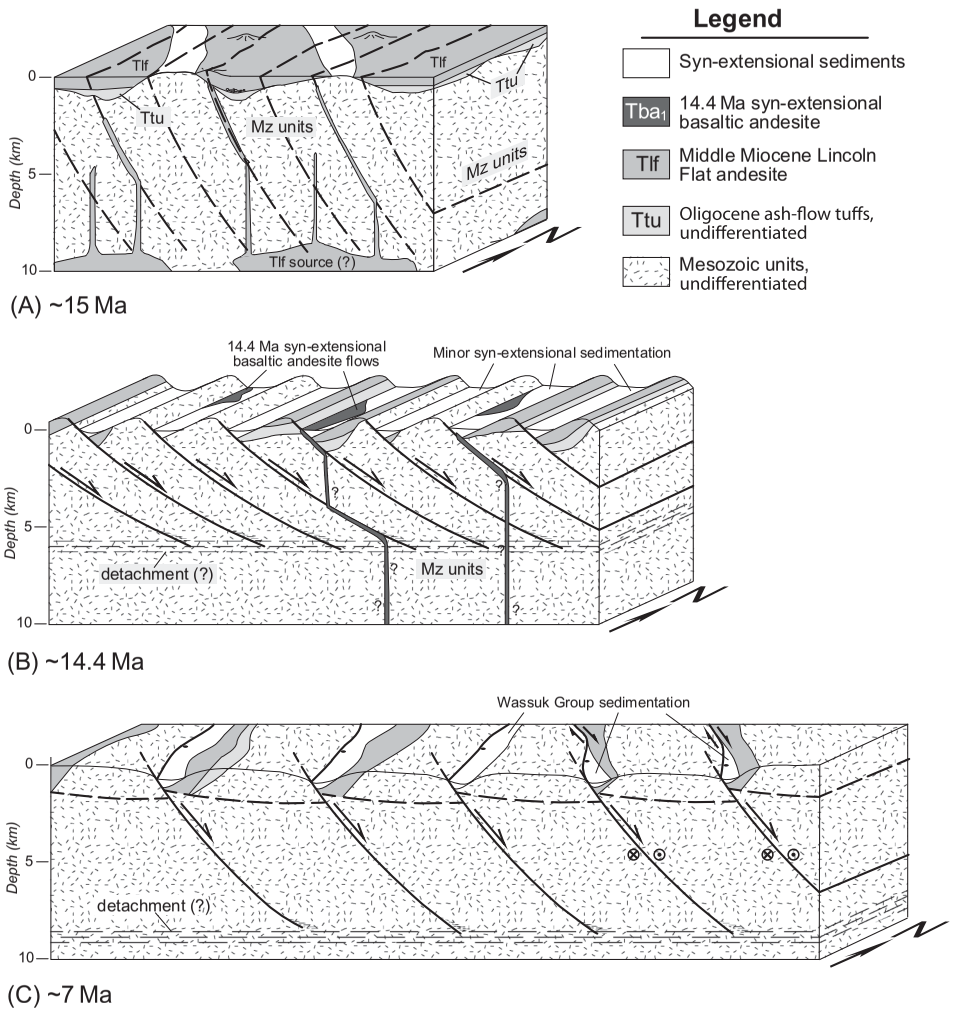

Figure 7. Schematic block diagrams displaying the structural and magmatic evolution of the central Wassuk Range from ~15 Ma to ~7 Ma. (A) Diagram displaying the distribution of both the Lincoln Flat andesite (map unit Tlf) and older Oligocene ash-flow tuffs (Ttu) at ~15 Ma, after the extrusion of most andesite flows. The early stages of closely spaced normal faulting that affected the area are also shown, with the latest extrusion of andesite utilizing the planes of weakness provided by fault planes, as documented by Dilles (1993) in the northern Wassuk Range. The depth of magma chambers that were the source for these andesite flows is not known, but there is no evidence for the intrusive equivalent of map unit Tlf at levels shallower than 8 km in the Wassuk Range fault block (Figure 3). (B) Diagram displaying the first set of high-angle normal faults after approximately 25° of westward fault block rotation at 14.4 Ma, constrained by the orientation of volumetrically minor basaltic andesite flows. Faults are shown here as gently listric (1°–2° change in dip/km depth), soling into a possible detachment horizon. (C) Diagram displaying second generation of more widely spaced, gently listric, high-angle normal faults cutting and displacing the now inactive first generation of normal faults at ~7 Ma. The diagram shows approximately 10° of block rotation accommodated by the second generation of normal faults. In this interpretation, the second generation of faults became active when the first generation of faults had rotated to approximately 30° eastward dip. See Figure 3 for present-day cross-section.

Downloaded By: [Surpless, Benjamin E.] At: 14:16 19 April 2011

the initiation of normal faulting. In addition, it is likely that there was a thick, relatively cool crust beneath the study area at the onset of this time period (e.g. Coney and Harms 1984; Severinghaus and Atwater 1990), with the eruption of these Oligocene tuffs likely signalling the beginning of a very gradual warming and weakening of the crust beneath western Nevada that continued until the onset of major extension. Prior to the eruption of these tuffs, it is likely that the geothermal gradient beneath the area was similar to the early Tertiary geothermal gradient of 10 ± 5°C/km for the nearby Sierra Nevada (Dumitru 1990), much cooler than the present-day geothermal gradient of 30°–35°C/km (e.g. Lachenbruch and Sass 1980).

After an ~11 Ma hiatus in volcanism, the Lincoln Flat andesite (Tlf) was erupted at ~15 Ma in the central Wassuk Range study area. The striking similarity between the geochemistry of older Jurassic and Cretaceous plutons, emplaced during normal west-facing subduction, and the trace-element signatures of ~15 Ma andesite samples (Figure 5C) suggest that these flows signalled the re-establishment of normal, west-facing subduction beneath western North America at this latitude. The timing is consistent with the large volumes of andesitic lavas that were extruded in eastern California, western Nevada, central Oregon, and Central Washington between 20 Ma and 10 Ma (Lipman 1992; Figure 1), with the cessation of this magmatism migrating northward in concert with the initiation of dextral motion along the San Andreas Fault system (e.g. Christiansen *et al.* 1992).

The ~15 Ma flows display variations in strike direction that likely reflect the mantling of pre-existing topography (Figure 3). On the western margin of the Grey Hills block (Figure 3), a major palaeovalley had been established by ~15 Ma, with Lincoln Flat andesite flows deposited in a palaeovalley cut through the Oligocene map units and into the Mesozoic basement. This finding is consistent with NW-trending river palaeovalleys in the Singatse Range to the west (Figure 2) (Proffett and Proffett 1976). The lack of any significant conglomerate or other sedimentary rocks underlying the basal flows of the Lincoln Flat andesite suggests that area-wide uplift and/or erosion continued throughout this period.

There are small to negligible differences between dips of the Oligocene silicic ash-flow tuffs and overlying andesite flows, suggesting that little or no extension occurred in the central Wassuk Range between about 26 Ma and 15 Ma. This is consistent with field relationships in the Singatse and Buckskin ranges (Figure 2), where there is no significant angular discordance between Oligocene tuffs and Miocene andesites (Dilles and Gans 1995). Although normal faulting may have initiated before 15 Ma (e.g. Dilles 1993; Dilles and Gans 1995), there is no evidence for significant faulting during this period in the study area, and apatite fission-track and (U–Th)/He data show little or no cooling related to footwall uplift during this time (Stockli *et al.* 2002).

Heating of the crust associated with this middle Miocene magmatism is thought to be an important factor in the initiation of the large-magnitude extensional event that began immediately after the eruption of the Lincoln Flat andesite (Stockli *et al.* 2002), similar to models that closely tie magmatism to the initiation and development of extensional terranes (e.g. Gans *et al.* 1989; Lister and Baldwin 1993; Parsons and Thompson 1993). Figure 6A displays a possible setting for the initiation of extension, with magmas at depth thermally weakening the upper crust, potentially providing an initial area of weakness for shear associated with a detachment surface at the base of the closely spaced fault blocks (shown after the initiation of extension in Figure 6B). However, plutonic equivalents of Lincoln Flat andesite flows are not exposed in the field area, so the depth of the magma chambers shown on the diagram is conjectural.

15–12 Ma time interval

Low-temperature thermochronologic data from transects across the Grey Hills and Wassuk blocks (Figure 3) (Stockli *et al.* 2002) suggest that the initiation of rapid extension immediately followed the extrusion of the Lincoln Flat andesite flows at 15 Ma. The field relationship between flows of the ~15 Ma Lincoln Flat andesite, with ~60° westward dips, and the ~14.4 Ma basaltic andesite flow, with a 35° westward dip, supports this timing, suggesting that at least ~25° of westward tilting was accommodated during the first ~0.6 Ma of faulting (Figure 6B). It is likely that the volumetrically minor basaltic andesite magmas utilized fault planes to reach the surface (Figure 6B), based on the location of the exposed flow relative to the known first-generation fault location. The 8.7 mm/year strain rate, based on palinspastic restoration and geochronology, is similar to some of the highest rates of extension documented in the Basin and Range (e.g. Dilles and Gans 1995; Gans *et al.* 2001).

The first generation of normal faults, active during this period, today dips very shallowly to the east to subhorizontal, at an angle of approximately 65° from the present-day attitudes of bedding offset by these faults (the best exposure of this generation is at the northern margin of the Buck Brush Spring block in Figure 3). Based on the bedding–fault relationships, the first generation of normal faults was initiated at high angles (60°–70°) throughout the study area. These data are consistent with middle Miocene andesite dikes (map unit Tlf) that cut Jurassic intrusions in the western part of the study area, strike N–NW, and dip 30°–35° to the east (one such dike is shown in Figure 3), and planar zones of intense Jurassic sodic and sodic-calcic alteration that now dip 25°–30° to the east.

Assuming the dikes and zones of alteration were intruded vertically, these dips are also consistent with 55°–60° rotation of the first generation of east-dipping normal faults.

These faults are most responsible for the three major repetitions of the steeply west-dipping Tertiary volcanic sequence and Tertiary unconformity (Figures 3 and 7). The timing of the initiation of the second generation of normal faults, which dip at moderate angles today (Figure 3) is not as well constrained as the first generation, but palinspastic restoration of extension suggests that the first generation of normal faults is responsible for most extension in the central Wassuk Range, suggesting that the first generation of faults remained active to relatively low angles (<30°) during this time period. In this interpretation, the first generation of faults rotated approximately 35° from the angle of initiation before the second generation of faults became active (Figure 7), and the level of the detachment rose in the crust from approximately 10 km depth to 6–7 km, which would significantly increase the local geothermal gradient and lead to cooling of the rocks present within the detachment itself.

Apatite fission-track and (U–Th)/He data indicate that rapid exhumation related to faulting and footwall uplift continued until about 12 Ma (Stockli *et al.* 2002). These data indicate a geothermal gradient of 28° ± 5°C/km at the onset of extension (Stockli *et al.* 2002), significantly higher than the early Tertiary geothermal gradient of 10° ± 5°C/km in the nearby Sierra Nevada (Dumitru 1990), but lower than the modern geothermal gradient of 30°–35°C/km (e.g. Lachenbruch and Sass 1980). Although eruption of the Lincoln Flat andesite immediately preceded faulting, no volumetrically significant volcanic rocks are known to have erupted in the study area during rapid extension (15 Ma and 12 Ma), a phenomenon observed elsewhere in the Basin and Range province (Meyer and Foland 1991; Sawyer *et al.* 1993; Dilles and Gans 1995; Spencer *et al.* 1995; Gans and Bohrson 1998). Gans and Bohrson (1998) hypothesize that major normal faulting enhances crystallization of potential lavas at depth by a range of possible mechanisms, including exsolution of volatiles and crystallization due to decrease in confining pressure, crystallization due to meteoric water–magma interaction promoted by faulting, or segregation of large magma bodies by motion along shear zones, thus promoting more rapid cooling and crystallization.

The similarities between the episode of middle Miocene extension in the Wassuk Range and that documented in the nearby Yerington District of the Singatse Range are striking and suggest an area-wide episode of rapid extension (Figure 2). In both cases, extension was accommodated by multiple generations of normal faults and was likely permitted by the addition of heat to the crust by voluminous pre-extensional magmatism. In both locations, the first generation of normal faults was closely spaced (1–2 km), was initiated at high angles, and accommodated most extension. The second generation of faults accommodated minor fault block rotation, and the third set of faults (still active in many cases) has accommodated 8°–12° of fault block rotation (Proffett 1977; personal communication, J. Dilles, 1998; this study). The total extension in both the central Wassuk Range and the Singatse Range is likely greater than 200% (personal communication, J. Dilles, 1998; this study), and strain rates were likely between 5 mm/year and 10 mm/year during the highest rates of extension (Dilles and Gans 1995; this study).

12–4 Ma time interval

The sudden decrease in rates of footwall cooling and uplift related to extension at approximately 12 Ma (Stockli *et al.* 2002) might be tied to a change in thermal structure of the upper crust, with isotherms relaxing after the highest rates of extension, thus increasing the strength of the upper crust. Between 12 Ma and 4 Ma, extension continued at a much lower rate, accommodated primarily by a second generation of initially high-angle, NNW-striking, east-dipping, dip-slip to oblique-dextral-slip normal faults in the central Wassuk Range (Figure 3). Today, this second generation of faults dips at moderate angles (25°–40°) and appears to have been active coeval with deposition of the syn-extensional Wassuk Group (map unit Tws). The cross-cutting relations between the first and second generations of normal faults are poorly constrained in the map area because there is no good exposure of the interaction of the two fault generations.

In the schematic structural interpretation shown in Figure 7B, the second generation of faults is interpreted to have cut and displaced the first generation faults after approximately 35° rotation. This relationship is similar to that documented in the Singatse Range to the west (Proffett and Proffett 1976; Proffett and Dilles 1984). However, on the western margins of the Grey Hills, Buck Brush Spring, and Wassuk blocks, the second generation of faults is proximal to the surface exposure of the first generation of normal faults that accommodated most of the extension in the area, suggesting an intimate relationship between the first and second generations of faults, with the second generation of faults possibly transferring slip onto the low-angle first-generation fault surfaces at depth, merging with the older faults, similar to the interpretation of Brady *et al*. (2000) for the Singatse Range to the west. In either case, the second generation of normal faults did not accommodate a significant percentage of the total extension documented in the field area. Low-temperature thermochronologic data support field data, suggesting that the magnitude of westward tilting of major fault blocks in most of the study area between ~8.6 Ma and ~4 Ma is probably relatively small (Stockli *et al.* 2002).

Downloaded By: [Surpless, Benjamin E.] At: 14:16 19 April 2011

Downloaded By: [Surpless, Benjamin E.] At: 14:16 19 April 2011

Importantly, dextral deformation was also initiated during this time period, with the dextral strike–slip faults in the study area, including the Reese River and Buck Brush Spring faults (Figure 3), responsible for the only significant dextral deformation documented west of the present-day, east-dipping Wassuk Range normal fault system (Figure 2). Dextral faults in the study area are subparallel to the active dextral faults of the Walker Lane to the east (Figure 2). The Buck Brush Spring fault accommodated approximately 2350 m of apparent dextral displacement, based on offset of the Tertiary unconformity (this study), whereas the Reese River fault accommodated approximately 3350 m of dextral displacement (McIntyre 1990). If all motion along these faults was approximately coeval with deposition of the Wassuk Group, between ~9 Ma and ~7 Ma in the study area (McIntyre 1990), then the slip rates along these faults would be of the order of 1.2 mm/year for the Buck Brush Spring fault and 1.7 mm/year for the Reese River Canyon fault, comparable to the highest rates of slip along modern Walker Lane faults to the east (e.g. Wesnousky 2005). The geometric relationship between the two Wassuk Group depocenters and these two dextral faults (Figures 3 and 7C) might indicate that dextral faulting was the dominant mode of deformation during this period.

Although workers to the north (Mohawk Valley fault zone, north of Lake Tahoe; e.g. Hawkins *et al.* 1986; Sawyer and Briggs 2001) and south (White Mountains; Stockli *et al.* 2003) of the study area have documented a westward migration of dextral deformation that continues to the present, movement along dextral faults affecting the central Wassuk Range ceased by about 7 Ma (McIntyre 1990), and there is no evidence that any significant strike–slip deformation has affected the region to the west of the Wassuk Range since that time (e.g. Surpless *et al.* 2002).

After the eruption of the ~14.4 Ma basaltic andesite flow, no volcanic rocks were erupted in the central Wassuk Range until the time of Wassuk Group deposition at ~9.5 Ma (McIntyre 1990; Dilles 1993; this study). With the exception of the biotite-bearing air-fall tuff documented by McIntyre (1990), all volcanic rocks erupted in the study area during this period consisted of basaltic andesite flows. All samples from these flows display geochemical signatures similar to middle Miocene andesites and the older Cretaceous and Jurassic plutonic rocks in the study area (Figure 5D), suggesting no significant change in the mantle source area or the relative amount of crustal involvement in the evolution of magmas throughout Miocene time.

4 Ma to present

Thermochronologic data constrain the onset of significant extension-related cooling to a period since ~4 Ma (Stockli *et al.* 2002), so it is likely that most of the tilting documented in the ~7 Ma basaltic andesite flows and dikes (Tba_2) occurred since ~4 Ma. In most of the study area, the ~7 Ma basaltic andesite flows (McIntyre 1990; map unit Tba) exhibit westward tilts of 8°–12° (Figure 3), and a significant number of basaltic andesite dikes in the Wassuk block, tentatively correlated with the basaltic andesite flows, strike NNW and display 75°–85° eastern dips (Figure 3). Assuming the dikes were intruded as vertical planes, these data would indicate 5°–15° westward tilting of the Wassuk block about a horizontal axis oriented NNW since dike emplacement, consistent with the basaltic andesite flows.

The only prominent, active high-angle faults in the study area are those that make up the east-dipping fault system along the east flank of the Wassuk Range (Figure 3). Field inspection reveals brecciation and diffuse zones of cataclastic deformation (up to tens of metres wide) with extensive exposure of slickensides along much of the active fault system, which cuts late Pleistocene alluvial fan and bajada deposits (Bingler 1978) as well as Holocene deposits (Demsey *et al.* 1988). Calculations based on thermochronologic data suggest 2.5 ± 0.5 km of dip-slip offset along the range-front fault system since about 4 Ma (Stockli *et al.* 2002). Recent movement along faults of the range-front system is recorded in the rugged topography of the range and historic seismicity in the area (e.g. Rogers *et al.* 1991). Other, apparently inactive, high-angle (>50°) faults between the Grey Hills, Buck Brush Spring, and Wassuk blocks display only minor offsets (Figure 3).

Figure 3 shows the general N–NW strike and 65°–70° dip of fault planes along much of the range-bounding fault system in the central Wassuk Range. Brittle normal faults are initiated at these angles, so these fault planes and fault-slip indicators are reasonable indicators of the present-day tectonic regime. Lineation measurements display some scatter in motion direction, with many slickensides that indicate an oblique (dextral) sense of fault movement (Figure 3). Based on slip indicators, the present-day maximum extension direction is oriented approximately N75°W (Figure 3), consistent with modern geodetic data (Kreemer and Hammond 2007; Kreemer *et al.* 2009). These fault motion indicators echo contemporary strain measurements along the western margin of the northern Basin and Range (e.g. Zoback 1989; Dilles and Gans 1995; Schweickert *et al.* 2000) and suggest that there has been a clockwise rotation of the direction of maximum strain from E–W to WSW–ENE during the Miocene to WNW–ESE from the late Pliocene to the present.

In addition to the rotation of strain axes, the geochemical signature of Pliocene (?) or younger basaltic dikes exposed in the study area (Figure 5E) suggests a significant change in the generation and evolution of magmas beneath the study area. The depleted nature of these magmas suggests two non-exclusive possibilities: (1) the thickness of the brittle upper crust was reduced by Miocene extension, permitting easier rise of magmas through the crust in Pliocene or later time without significant crustal

contamination; and/or (2) the composition of the mantle source for magmas could have changed.

Discussion

Oligocene silicic volcanism likely signalled the onset of thermal weakening of thick, cool granitoid crust of the former Sierra Nevada batholith (Figure 1; e.g. Coney and Harms 1984; Severinghaus and Atwater 1990). Henry *et al*. (2009) suggest that the extraordinary distances that 31–23 Ma ash-flow tuffs travelled was possible due to the focused flow of these tuffs in palaeovalleys that drained westward toward the Pacific Ocean. These deep (0.5–1.5 km), broad (commonly 8–10 km) valleys were separated by low-relief topographic highs, consistent with the hypothesized high plateau present throughout much of Nevada and eastern California in the mid-Cenozoic (Henry *et al.* 2009). The chemistry of these silicic volcanic rocks in the study area suggests significant crustal contamination, which would be expected with a thick crust without easy pathways to the surface.

This thermal weakening of the crust continued with the eruption of voluminous Miocene andesite flows throughout the region, with the study area likely on the axis of the ancestral Cascades arc (Figure 1). Although extension immediately followed the eruption of these lavas, it is likely that the boundary conditions placed on the region by west-facing subduction were as important to the initiation of extension as the addition of heat to the middle and upper crust by rising magmas, based on the widespread initiation of extension ca. 19–14 Ma throughout the Basin and Range province (e.g. Miller *et al.* 1999; Stockli 1999; Colgan *et al.* 2008; Fosdick and Colgan 2008; Gonsoir and Dilles 2008). The chemistry of these Miocene andesites supports lesser crustal contamination than that experienced by earlier magmas, possibly indicating a thinner crust beneath the area relative to the Oligocene.

Middle Miocene extension was accommodated primarily by closely spaced (1–2 km), high-angle normal faults that rotated as extension progressed, possibly aided by a low-angle detachment surface at depth. Magma chambers for the andesitic lavas that were between 8 km and 10 km depth would have thermally weakened the surrounding rock, perhaps permitting ductile deformation and shearing along the base of the fault blocks formed by the first generation of normal faults (Figure 7B). As extension progressed after 15 Ma, any detachment zone at 8–10 km depth would necessarily move upward in the crust, cooling as the normal fault angles became shallower. Thus, cooling related to extension likely increased the competence of the former detachment zone, decreasing the likelihood that the detachment would remain active. At the same time, a decrease in fault angle would decrease the resolved shear stresses along the fault planes as normal stresses increased, decreasing the likelihood of continued movement at angles below 30°. Therefore, it is likely that rapid extension ceased in part due to the physics of fault motion.

If the hypothesized suppression of magmatism during the highest rates of extension is correct (e.g. Gans and Bohrson 1998), then the crystallization of magmas at depth would likely have occurred during this period. Without the significant addition of new magmas adding heat to the middle and upper crust from below, the strength of the crust would increase not only due to the relaxation of isotherms following the highest rates of extension (e.g. Stockli *et al.* 2002) but also due to the loss of magmatic heating from below. Thus, it would be unlikely that a second generation of normal faults would have permitted extension to continue at high rates even if the stress field remained basically unchanged.

From 12 Ma until 4 Ma, the rate of cooling related to extension was relatively low in the central Wassuk Range (Stockli *et al.* 2002). During this period, extensional deformation migrated to the west, affecting the Pine Nut Mountains, the Carson Range, and the area to the west of Lake Tahoe (Figure 2; e.g. Dilles and Gans 1995; Surpless *et al.* 2002; Cashman *et al.* 2009), potentially related to changes in the thermal structure of the crust (e.g. Surpless *et al.* 2002). Although the timing of the initiation of the second generation of normal faults is poorly constrained in the study area, these faults were clearly active during Wassuk Group sedimentation from ~9.5 Ma to 7 Ma. The wider spacing of faults relative to the first generation (4–6 km) appears to be influenced by the position of the first generation of faults (Figures 3 and 7C), suggesting either a direct kinematic relationship (e.g. Brady *et al.* 2000) or a pre-existing zone of weakness in the uppermost crust adjacent to the surface exposure of the first generation, permitting the downward propagation of faults and the establishment of the second generation of faults.

During this period from 12 Ma to 4 Ma, products of volcanic eruptions indicate no significant change in the source or evolution of these magmas. However, dextral deformation was initiated in the study area at about 9 Ma, coincident with the acceleration of dextral deformation along the central Walker Lane (Hardyman and Oldow 1991; Dilles and Gans 1995), and immediately following the first independent motion of the Sierra Nevada microplate at ~10 Ma (e.g. Saleeby *et al.* 2009). This was closely followed by the northward passage of the Mendocino triple junction (MTJ) at this latitude (Atwater and Stock 1998). As the MTJ migrated northward, both the San Andreas Fault system and the Walker Lane lengthened with lesser total displacements toward the north (e.g. Faulds *et al.* 2005). Thus, the acceleration in dextral fault activity in the central Walker Lane and the initiation of dextral faults cutting through the Wassuk Range is compatible with several factors affecting much of the western margin of the North American continent.

Downloaded By: [Surpless, Benjamin E.] At: 14:16 19 April 2011

Downloaded By: [Surpless, Benjamin E.] At: 14:16 19 April 2011

In contrast, the cessation of dextral faulting by ~7 Ma in the central Wassuk Range is not associated with any significant change in tectonic setting, but could be related to changes in the thermal structure of the crust in the field area. The Wassuk Range accommodated a component of the dextral strain associated with the acceleration of Walker Lane deformation starting at around 9 Ma, but continued cooling and strengthening of the middle and upper crust may have ended this dextral motion by ~7 Ma.

Since ~4 Ma, the footwall of the Wassuk fault block has experienced significant cooling related to extension accommodated by the range-front system (Stockli *et al.* 2002). The timing of the initiation of this increased rate of uplift in the central Wassuk Range is consistent with the work of Murphy *et al*. (2009), who hypothesize that a significant change in the kinematics of deformation across the central and southern Walker Lane might be related to the delamination of the lithospheric root of the southern Sierra Nevada at ~3 Ma (e.g. Gilbert *et al.* 2007).

Tied to this relatively recent increase in rate of uplift along the Wassuk Range normal fault system is the intrusion of basaltic dikes with depleted geochemical signatures. Although a change in the thickness and therefore strength of the brittle middle-upper crust might provide easier pathways to the surface, the chemistries of late Miocene basaltic andesite flows (interbedded flows in the Wassuk Group and map unit Tba_2) display no significant change in composition relative to pre-extensional Lincoln Flat andesite flows (Figure 5). Therefore, although a thinner crust experiencing extension likely provided pathways for these basalts to reach the surface, the significant depletion displayed on trace-element diagrams suggests that the mantle source of these magmas changed, perhaps from a subduction-related source to a source closer to MORB composition. This change might be explained by the northward migration of the Mendicino triple junction, growth of the San Andreas Fault, and cessation of arc-related magmatism. Furlong and Schwartz (2004) hypothesize passive asthenospheric inflow beneath the region formerly underlain by the Gorda slab. This mechanism might provide both a different source for magmas in the study area and thermal heating that might have weakened the western margin of the Basin and Range province at this latitude, permitting the previously described ~4 Ma pulse of footwall cooling related to extension in the central Wassuk Range, documented by Stockli *et al*. (2002).

The delay between passage of the MTJ and this pulse of extension and intrusion of basaltic dikes is compatible with the work of Dickinson (1997), who showed a ~3 Ma delay between passage of the MTJ and the eruption of volcanics in the Northern Coast Ranges (Figure 1), where the depth of the subducting Gorda Plate had been much shallower than beneath the Wassuk Range study area. Liu and Furlong (1992) attributed the delay between MTJ passage and volcanic eruptions to the time necessary to develop the subsurface magmatic system, but Furlong and Schwartz (2004) suggest the time lag might be attributed instead to the timing of mantle inflow into the slab window. For either explanation, the greater the depth of the Gorda Plate beneath the region, the longer the expected delay between passage of the MTJ and any detected change in tectonics and magmatism in the upper crust.

Interestingly, the trace-element patterns of basalts and basaltic andesites from the Northern Coast Ranges erupted as part of this process (Whitlock *et al.* 2001; Whitlock, 2002) closely match the patterns of Cascade arc volcanic rocks, suggesting that Coast Range volcanics were sourced from the same asthenospheric mantle wedge material as Cascade volcanoes (Furlong and Schwartz 2004). Furlong and Schwartz (2004) hypothesize that the mantle filling the slab window beneath the Coast Ranges is derived from the mantle wedge to the east, made of the same materials sourced by volcanoes of the Cascades. However, beneath the Wassuk Range region, the subducting slab would have been much deeper, and as the MTJ passed towards the north, the more likely source for inflowing mantle would come instead from below the former slab, providing new material largely unaffected by ongoing subduction processes. This material would likely be less hydrous and have higher temperature than mantle material from the former wedge (e.g. Furlong and Schwartz 2004), the likely source for all earlier Cenozoic volcanics in the central Wassuk Range.

Since ~4 Ma, the range-front fault system of the central Wassuk Range has continued to evolve in an extensional stress field, not significantly affected by the dextral deformation of the dominant Walker Lane faults to the east (Figure 2). Although other high-angle normal faults are present in the study area (Figure 3), none of these faults exhibit significant dip-slip displacement or any other features that might indicate Quaternary motion. Therefore, the significant historical seismicity along the east-dipping Wassuk Range front fault system, palaeoseismic studies that have documented large-magnitude (>M7.0) Holocene earthquakes associated with the system (e.g. Demsey 1987; Wesnousky 2005), and the morphology of the range-front fault system suggest that most if not all extension across the study area has been accommodated by that system since ~4 Ma.

Conclusions

In spite of modern geodetic data that suggest a systematically distributed dextral strain field across the western margin of the Basin and Range province (e.g. Dixon *et al.* 1995; Kreemer *et al.* 2009) and geologic data that demonstrate the complex nature of Walker Lane deformation (e.g. Gilbert and Reynolds 1973; Dilles and Gans 1995; Lerch *et al.* 2004), data presented here support a Cenozoic

geologic history for the central Wassuk Range dominated by extension accommodated primarily by dip-slip normal faults and likely controlled by a combination of changes in the thermal structure of the crust and regional tectonics. Deformation in the study area can be divided into three periods.

(1) Rapid middle Miocene extension immediately preceded by voluminous andesitic magmatism along the axis of the ancestral Cascade arc. This extension was accommodated by a fault system initiated at high angles to bedding and appears to be closely related to the combined thermal weakening of the crust and change in boundary conditions that affected much of the Basin and Range.
(2) Motion of dextral strike–slip and oblique normal-dextral slip faults between ~9.5 Ma and 7 Ma was likely related to the northward growth of the San Andreas Fault system and the northward passage of the MTJ. Although documented both north and south of the study area, westward migration of dextral deformation has not occurred at the latitude of the central Wassuk Range; all dextral fault motion ended at 7 Ma. Minor basaltic andesite volcanism with arc-related geochemical signatures took place during this period. Rates of extension remained low until ~4 Ma.
(3) From ~4 Ma to the present, nearly all deformation in the central Wassuk Range has been focused along the east-dipping range-bounding fault system, where extension continues today, proximal to the strike–slip faults of the central Walker Lane to the east. This renewed period of accelerated extension might also be related to the northward migration of the MTJ, where mantle upwelling into the slab window south of the Gorda Plate provided a significantly more depleted source for basaltic dikes that intruded the Wassuk fault block. The time lag between passage of the MTJ and the acceleration in rates of extension could be related to the rate of mantle upwelling and/or the time necessary to establish magmatic pathways to the surface. Today, the range-bounding fault system continues to accommodate extension and remains one of the most seismically active fault systems in the Basin and Range.

Thus, although the large-magnitude extensional event in the middle Miocene appears to be a relatively local event on the western margin of the Basin and Range province, all periods and modes of deformation (i.e. periods of extension and dextral deformation) in the central Wassuk Range were likely intimately related to plate boundary processes that affected much of the western margin of the North American continent.

Downloaded By: [Surpless, Benjamin E.] At: 14:16 19 April 2011

Acknowledgements

Thanks especially to Joe Colgan and Anne Egger for thorough reviews of the initial draft of this manuscript. Thanks also to Danny Stockli and Elizabeth Miller for helpful commentary. Thanks to Marco Einaudi and John Dilles for their helpful discussions about the structural complexities in the central Wassuk Range and the Singatse Range. Thanks also to George Thompson for his fruitful discussions about crustal scale deformation. Thanks to Michael McWilliams and Laura Webb for their cooperation and for the use of their $^{40}Ar/^{39}Ar$ laboratory at Stanford University. Costs associated with INAA analyses were covered by the US Department of Energy's University Reactor Sharing Grant to Oregon State University. Field work, transportation costs, and laboratory analyses were supported by the Stanford University McGee Fund, the Stanford University Shell Fund, and the US Geological Survey's EDMAP programme. This project was also supported in part by NSF grants EAR-9417939 and EAR-9725371 awarded to Elizabeth Miller and Trevor Dumitru.

References

Armstrong, P.A., Ehlers, T.A., Chapman, D.S., Farley, K.A., and Kamp, P.J., 2003, Exhumation of the central Wasatch Mountains, Utah: 1. Patterns and timing of exhumation deduced from low-temperature thermochronology data: Journal of Geophysical Research, v. 108, no. B3, p. 2172, doi: 10.1029/2001JB001708.

Atwater, T., and Stock, J., 1998, Pacific-North America plate tectonics of the Neogene Southwestern United States – an update: International Geological Review, v. 40, p. 375–402.

Battles, D.A., 1990, The hydrothermal evolution of the Shamrock batholith, western Nevada, and the origin of sodium-rich alteration in western United States[unpublished Ph.D. thesis]: Los Angeles, University of California.

Battles, D.A., 1991, Hydrothermal alteration within the tilted Shamrock batholith, Yerington District, Nevada, *in* Raines, G.L., Lisle, R., Schafer, R.W., and Wilkinson, W.H., eds., Geology and ore deposits of the Great Basin; Symposium proceedings: Reno, NV, Geological Society of Nevada, p. 351–353.

Bennett, R.A., Davis, J.L., and Wernicke, B.P., 1999, Present-day pattern of Cordilleran deformation in the western United States: Geology, v. 27, no. 4, p. 371–374.

Bingler, E.C., 1978, Geologic map of the Shurz quadrangle: Reno, NV, Nevada Bureau of Mines and Geology Map 60.

Bormann, J., Wesnousky, S., Hammond, B., and Sarmiento, A., 2010, Holocene earthquakes along the Wassuk range fault zone: Paleoseismic observations from the Rose Creek Fan, Hawthorne, Nevada, USA: Geothermal Resources Council Transactions, v. 34.

Brady, R.J., Wernicke, B.P., and Fryxell, J.E., 2000, Kinematic evolution of a large-offset continental normal fault system, South Virgin Mountains, Nevada: Geological Society of America Bulletin, v. 112, no. 9, p. 1375–1397.

Burchfiel, B.C., Cowan, D.S., and Davis, G.A., 1992, Tectonic overview of the Cordilleran Orogen in the Western United States, *in* Buchfiel, B.C., Lipman, P.W., and Zoback, M.L., eds., The Cordilleran Orogen: Conterminous United States, Volume G3: Geology of North America: Boulder, Geological Society of America, p. 407–479.

Cashman, P.H., Trexler, J.H., Jr., Muntean, T.W., Faults, J.E., Louie, J.N., and Oppliger, G.L., 2009, Neogene tectonic evolution of the Sierra Nevada–Basin and Range transition zone at the latitude of Carson City, Nevada, *in* Oldow, J., and

Cashman, P., eds., Late Cenozoic structure and evolution of the Great Basin–Sierra Nevada transition: Geological Society of America Special Paper 447, p.171–188.

Christiansen, R.L., Yeats, R.S., Graham, S.A., Niem, W.A., and Snavely, Jr., P.D., 1992, Post-Laramide geology of the U.S. cordilleran region, *in* Burchfiel, B.C., Lipman, P.W., and Zoback, M.L., eds., The Cordilleran Orogen: Conterminous United States, Volume G3: Boulder, Geological Society of America, p. 261–406.

Colgan, J.P., Dumitru, T.A., McWilliams, M.O., and Miller, E.L., 2006, Timing of Cenozoic volcanism and Basin and Range extension in northwestern Nevada: New constraints from the northern Pine Forest Range: Geological Society of America Bulletin, v. 118, no. 1/2, p. 126–139.

Colgan, J.P., John, D.A., Henry, C.D., and Fleck, R.J., 2008, Large-magnitude Miocene extension of the Eocene Caetano caldera, Shoshone and Toiyabe Ranges, Nevada: Geosphere, v. 4, p. 107–130.

Coney, P.J., and Harms, T., 1984, Cordilleran metamorphic core complexes: Cenozoic extensional relics of Mesozoic compression: Geology, v. 12, no. 9, p. 550–554.

Cowan, D.S., and Bruhn, R.L., 1992, Late Jurassic to early Late Cretaceous geology of the U.S. Cordillera, *in* Burchfiel, B.C., Lipman, P.W., and Zoback, M.L., eds., The Cordilleran orogen: Conterminous United States, Volume G3: Boulder, Geological Society of America, p. 169–204.

Demsey, K., 1987, Late Quaternary faulting and tectonic geomorphology along the Wassuk Range, west-central Nevada: Geological Society of America Abstracts with Programs, v. 19, p. 640.

Demsey, K.A., Pearthtree, P.A., and Fouty, S., 1988, Segmentation of faulting and relative tectonic activity along the Wassuk Range, west-central Nevada: Geological Society of America Abstracts with Programs, v. 20, p. 155.

Dickinson, W.R., 1997, Tectonic implications of Cenozoic volcanism in coastal California: Geological Society of America Bulletin, v. 109, p. 943–954.

Dilles, J.H., 1993, Cenozoic and normal and strike-slip faults in the northern Wassuk Range, western Nevada, *in* Craig, S.D., ed., Structure, tectonics, and mineralization of the Walker Lane; Walker Lane Symposium Proceedings: Reno, NV, Geological Society of Nevada, p. 114–136.

Dilles, J., and Gans, P.B., 1995, The chronology of Cenozoic volcanism and deformation in the Yerington area, western Basin and Range and Walker Lane: Geological Society of America Bulletin, v. 107, p. 474–486.

Dilles, J.H., and Wright, J.E., 1988, The chronology of early Mesozoic arc magmatism in the Yerington District of western Nevada and its regional implications: Geological Society of America Bulletin, v. 100, p. 644–672.

Dixon, T.H., Stefano, R., Lee, J., and Reheis, M.C., 1995, Constraints on present-day Basin and Range deformation from space geodesy: Tectonics, v. 14, p. 755–772.

Duffield, W.A., and Dalrymple, G.B., 1990, The Taylor Creek Rhyolite of New Mexico: A rapidly emplaced field of lava domes and flows: Bulletin of Volcanology, v. 52, p. 475–487.

Dumitru, T.A., 1990, Subnormal Cenozoic geothermal gradients in the extinct Sierra Nevada magmatic arc: Consequences of Laramide and post-Laramide shallow-angle subduction: Journal of Geophysical Research, v. 95, p. 4925–4941.

Eaton, G.P., 1982, The Basin and Range province: Origin and tectonic significance: Annual Review of the Earth and Planetary Sciences, v. 10, p. 409–440.

Eddington, P.K., Smith, R.B., and Reneggli, C., 1987, Kinematics of Basin and Range intraplate extension, *in* Coward, M.P., Dewey, J.F., and Hancock, P.L., eds., Continental extensional tectonics, Volume 28: Geological Society Special Publication, Geological Society, p. 371–392.

Ekren, E.B., and Byers, F.M., Jr., 1984, The Gabbs Valley Range – a well-exposed segment of the Walker Lane in west-central Nevada, *in* Lintz, J.R., ed., Western Geological Excursions: Geological Society of America Annual Meeting Fieldtrip Guidebook: Boulder, Geological Society of America, p. 203–215.

Ekren, E.B., Byers, E.M., Jr., Hardyman, R.F., Marvin, R.F., and Silberman, M.L., 1980, Stratigraphy, preliminary petrology, and some structural features of Tertiary volcanic rocks in the Gabbs Valley and Gillis Range, Mineral County, Nevada: U.S.G.S. Bulletin Number 1464, 54 p.

Faulds, J.E., Henry, C.E., Hinz, N.H., 2005, Kinematics of the northern Walker Lane – an incipient transform fault along the Pacific – North American plate boundary: Geology, v. 33, p. 505–508.

Fosdick, J.C., and Colgan, J.P., 2008, Miocene extension in the East Range, Nevada: A two-stage history of normal faulting in the northern Basin and Range: Geological Society of America Bulletin, v. 120, p. 1198–1213.

Furlong, K.P., and Schwartz, S.Y., 2004, Influence of the Menocino Triple Junction on the Tectonics of coastal California: Annual Reviews of Earth and Planetary Sciences, v. 32, p. 403–433.

Gans, P.B., and Bohrson, W.A., 1998, Suppression of volcanism during rapid extension in the Basin and Range province, United States: Science, v. 279, p. 66–68.

Gans, P.B., Mahood, G.A., and Schermer, L., 1989, Synextensional magmatism in the Basin and Range province: A case study from the eastern Great Basin: Boulder, CO, Geological Society of America, 53 p.

Gans, P.B., Seedorff, E., Fahey, P.L., Hasler, R.W., Maher, D.J., Jeanne, R.A., and Shaver, S.A., 2001, Rapid Eocene extension in the Robinson district, White Pine County, Nevada: Constraints from $^{40}Ar/^{39}Ar$ dating: Geology, v. 29, p. 475–478.

Garside, L., Henry, C.D., and Boden, D.R., 2002, Far-flung ash-flow tuffs of Yerington, western Nevada erupted from calderas in the Toquima range, central Nevada: Geological Society of America Fall Meeting, Paper No. 14–21.

Gilbert, H., Jones, C., Owens, T.J., and Zandt, G., 2007, Imaging Sierra Nevada lithospheric sinking: EOS (Transactions, American Geophysical Union), v. 88, p. 225, 229.

Gilbert, C.M., and Reynolds, D.R., 1973, Character and chronology of Basin development, western margin of the Basin and Range province: Geological Society of America Bulletin, v. 84, p. 2489–2509.

Glazner, A.F., and Bartley, J.M., 1984, Timing and tectonic setting of Tertiary low-angle normal faulting and associated magmatism in the southwestern United States: Tectonics, v. 3, p. 385–396.

Gonsoir, Z.J., and Dilles, J.H., 2008, Timing and evolution of Cenozoic extensional normal faulting and magmatism in the southern Tobin Range, Nevada: Geosphere, v. 4, doi: 10.1130/GES00137.1.

Hardyman, R.F., and Oldow, J.S., 1991, Tertiary tectonic framework and Cenozoic history of the central Walker Lane, Nevada, *in* Raines, G.L., Lisle, R.E., Schafer, R.W., and Wilkinson, W.H., eds., Geology and ore deposits of the Great Basin: Geological Society of Nevada, p. 184–199.

Hawkins, F.F., LaForge, R., and Hansen, R.A., 1986, Seismotectonic study of the Truckee/Lake Tahoe area,

Downloaded By: [Surpless, Benjamin E.] At: 14:16 19 April 2011

northeastern Sierra Nevada, California: Seismotectonic Report 85-4, Bureau of Reclamation, Denver, Colorado, 174 p.

Henry, C.D., Faulds, J.E., Hinz, N.H., Garside, L.J., and Boden, D.R., 2009, Implications of widespread, paleovalley-filling ash-flow tuffs of the western Great Basin for paleotopography, regional tectonics, and tuff volumes: Geological Society of America Abstracts with Programs, v. 41, p. 18.

Henry, C.D., Faulds, J.E., and dePolo, C., 2007, Geometry and timing of strike-slip and normal faults in the northern Walker Lane, northwestern Nevada and northeastern California; strain partitioning or sequential extensional and strike-slip deformation?, *in* Till, A.B., Roeske, S.M., Sample J.C., and Foster, D.A., eds., Exhumation associated with continental strike-slip fault systems: Geological Society of America Special Paper 434, p. 59–79.

John, D.A., 1992, Stratigraphy, regional distribution, and reconnaissance geochemistry of Oligocene and Miocene volcanic rocks in the Paradise Range and northern Pactolus Hills, Nye County, Nevada: U.S.G.S. Bulletin Number 1974, 67 p.

John, D.A., Schweickert, R.A., and Robinson, A.C., 1994, Granitic rocks in the Triassic-Jurassic magmatic arc of western Nevada and eastern California: Geological Society of America, Boulder, CO, 61 p.

Kreemer, C., Blewitt, G., and Hammond, W.C., 2009, Geodetic constraints on contemporary deformation in the northern Walker Lane: 2. Velocity and strain rate tensor analysis, *in* Oldow, J., and Cashman, P., eds., Late Cenozoic structure and evolution of the Great Basin – Sierra Nevada transition: Geological Society of America Special Paper 447, p. 17–32.

Kreemer, C., and Hammond, W.C., 2007, Geodetic constraints on areal changes in the Pacific–North America plate boundary zone: What controls Basin and Range extension?: Geology, v. 35, no. 10, p. 943–947.

Lachenbruch, A.H., and Sass, J.H., 1980, Models of an extending lithosphere and heat flow in the Basin and Range province, *in* Smith, R.B., and Eaton, G.P., eds., Cenozoic tectonics and regional geophysics of the western Cordillera, Volume 152: Geological Society of America Memoir: Boulder, CO, Geological Society of America, p. 209–250.

Lerch, D.W., McWilliams, M.O., Miller, E.L., and Colgan, J.P., 2004, Structure and magmatic evolution of the northern Black Rock Range, Nevada: Preparation for a wide angle refraction/reflection survey: Geological Society of America Abstracts with Programs, v. 36, no. 4, p. 37.

Lipman, P.W., 1992, Magmatism in the Cordilleran U.S.: Progress and problems, *in* Burchfiel, B.C., Lipman, P.W., and Zoback, M.L., eds., The Cordilleran Orogen: Conterminous United States, Volume G3: The Geology of North America: Boulder, Geological Society of America, p. 481–514.

Lister, G.S., and Baldwin, S.L., 1993, Plutonism and the origin of metamorphic core complexes: Geology, v. 21, p. 607–610.

Liu, M., and Furlong, K.P., 1992, Cenozoic volcanism in the California Coast Ranges: Numerical solutions: Journal of Geophysical Research, v. 97, p. 4941–4951.

McIntosh, W.C., Geissman, J.W., Chapin, C.E., Kunk, M.J., and Henry, C.D., 1992, Calibration of the latest Eocene-Oligocene geomagnetic polarity time scale using $^{40}Ar/^{39}Ar$ dated ignimbrites: Geology, v. 20, p. 459–463.

McIntyre, J., 1990, Late Cenozoic structure of the Central Wassuk Range, Mineral County, Nevada[unpublished MS thesis]: Corvallis, Oregon State University.

Meyer, J., and Foland, K., 1991, Magmatic-tectonic interaction during early Rio Grande Rift extension at Questa, New Mexico: Geological Society of America Bulletin, v. 103, p. 993–1006.

Miller, E.L., Dumitru, T.A., Brown, R.W., and Gans, P.B., 1999, Rapid Miocene slip on the Snake Range-Deep Creek Range fault system, east-central Nevada: Geological Society of America Bulletin, v. 111, p. 886–905.

Minster, J.B., and Jordan, T.H., 1987, Vector constraints on western U.S. deformation from space geodesy, neotectonics and plate motions: Journal of Geophysical Research, v. 92, p. 4798–4804.

Murphy, J.J., Watkinson, J., and Oldow, J., 2009, Spatially partitioned transtension within the central Walker Lane, western Great Basin, USA: Application of the polar Mohr construction for finite deformation, *in* Oldow, J.S., and Cashman, P.H., eds., Late Cenozoic Structure and Evolution of the Great Basin–Sierra Nevada transition: Geological Society of America Special Paper 447, p. 55–70.

Oldow, J.S., 2003, Active transtensional boundary zone between the western Great Basin and Sierra Nevada block, western U.S. Cordillera: Geology, v. 31, p. 1033–1036.

Oldow, J.S., Kohler, G., and Donelick, R.A., 1994. Late Cenozoic extensional transfer in the Walker Lane strike-slip belt, Nevada: Geology, v. 22, p. 637–640.

Parsons, T., and Thompson, G.A., 1993, Does magmatism influence low-angle normal faulting?: Geology, v. 21, p. 247–250.

Pearce, J.A., 1982, Trace element characteristics of lavas from destructive plate boundaries, *in* Thorpe, R.S., ed., Andesites: Orogenic andesites and related rocks: Chichester, Wiley, p. 525–548.

Pearce, J.A., 1983, Role of sub-continental lithosphere in magma genesis at active continental margins, *in* Hawkesworth, C.J., and Norry, M.J., eds., Continental basalts and mantle xenoliths: Nantwich, Shiva Publishing, p. 230–249.

Proffett, J.M., Jr., 1977, Cenozoic geology of the Yerington District, Nevada, and implications for the nature and origin of Basin and Range faulting: Geological Society of America Bulletin, v. 88, p. 247–266.

Proffett, J.M., Jr., and Dilles, J.H., 1984, Geologic map of the Yerington district, Nevada: Reno, NV, Nevada Bureau of Mines and Geology Map 77.

Proffett, J.M., Jr., and Proffett, B.H., 1976, Stratigraphy of the Tertiary ash-flow tuffs in the Yerington district, Nevada: Reno, NV, Nevada Bureau of Mines and Geology Report, p. 28.

Rogers, A.M., Harmsen, S.C., Corbett, E.J., Priestly, K., and dePolo, D., 1991, The seismicity of Nevada and some adjacent parts of the Great Basin, *in* Slemmons, D.B., Engdahl, E.R., Zoback, M.D., and Blackwell, D.D., eds., Neotectonics of North America, Geological Society of America, Decade Map 1.

Saleeby, J., Saleeby, Z., Nadin, E., and Maheo, G., 2009, Stepover in the structure controlling the regional west tilt of the Sierra Nevada microplate; eastern escarpment system to Kern Canyon system: International Geology Review, v. 51, p. 634–669.

Saunders, A.D., and Tarney, J., 1984, Geochemical characteristics of basaltic volcanism within back-arc basins, *in* Kokelaar, B.P., and Howells, M.F., eds., Marginal basin geology, Volume 16: London, Geological Society of London, p. 59–76.

Sawyer, T., and Briggs, R.W., 2001, Stop 9: Kinematics and late Quaternary Activity of the Mohawk Valley fault zone: Pacific Cell Friends of the Pleistocene 2001 Fall Field Trip Guidebook.

Sawyer, T.L., Wakabayashi, J., Page, W.D., Thompson, S.C., and Ely, R.W., 1993, Late Cenozoic internal deformation of

Downloaded By: [Surpless, Benjamin E.] At: 14:16 19 April 2011

the northern and central Sierra Nevada, California: A new perspective: EOS, AGU Transactions, v. 74, p. 609.
Schweickert, R.A., Lahren, M.M., Karlin, R., Smith, K.D., and Howle, J.F., 2000, Lake Tahoe active faults, landslides, and tsunamis, *in* Lageson, D., Peters, S., and Lahren, M.M., eds., Great Basin and Sierra Nevada: Geological Society of America Field Guide 2, p. 1–34.
Seedorff, E., 1991, Magmatism, extension, and ore deposits of Eocene to Holocene age in the Great Basin: Mutual effects and preliminary proposed genetic relationships, *in* Raines, G.L., Lisle, R.E., Schafer, R.W., and Wilkinson, W.H., eds., Geology and ore deposits of the Great Basin: Reno, NV, Geological Society of Nevada, p. 133–178.
Severinghaus, J., and Atwater, T., 1990, Cenozoic geometry and thermal state of the subducting slabs beneath western North America, *in* Wernicke, B.P., ed., Basin and Range extensional tectonics near the latitude of Las Vegas, Nevada, Volume Memoir 176: Boulder, Geological Society of America, p. 1–22.
Spencer, J.E., Richard, S.M., Reynolds, S.J., Miller, R.J., Shafiqullah, M., Gilbert, W.G., and Grubensky, M.J., 1995, Spatial and temporal relationships between mid-Tertiary magnetism and extension in southwestern Arizona: Journal of Geophysical Research, v. 100, p. 10321–10351.
Stewart, J.H., 1980, Regional tilt patterns of late Cenozoic basin-range fault blocks, western United States: Geological Society of America Bulletin, v. 91, p. 460–464.
Stewart, J.H., 1993, Walker Lane Belt, Nevada and California – An overview, *in* Craig, S.D., ed., Structure, tectonics, and mineralization of the Walker Lane; Walker Lane Symposium Proceedings: Reno, NV, Geological Society of Nevada, p. 1–16.
Stockli, D.F., 1999, Regional timing and spatial distribution of Miocene extension in the northern Basin and Range Province [Ph.D. thesis]: Stanford, CA, Stanford University, 239 p.
Stockli, D.F., Dumitru, T.A., McWilliams, M.O., and Farley, K.A., 2003, Cenozoic tectonic evolution of the White Mountains, California and Nevada: Geological Society of America Bulletin, v. 115, p. 788–816.
Stockli, D.F., Surpless, B.E., Dumitru, T.A., 2002, Thermochronological constraints on the timing and magnitude of Miocene and Pliocene extension in the central Wassuk Range, western Nevada: Tectonics, v. 21, no. 4, doi: 10.1029/2001TC001295.
Sun, S.S., 1980, Lead isotopic study of young volcanic rocks from mid-ocean ridges, ocean islands, and island arcs: Philosophical Transactions of the Royal Society, v. A297, p. 409–445.
Surpless, B.E., 1999, A structural, magmatic, and thermochronological study of the central Wassuk Range, western Nevada [Ph.D. thesis]: Stanford, CA, Stanford University, 225 p.
Surpless, B.E., 2008, Modern strain localization in the central Walker Lane, western United States: Implications for the evolution of intraplate deformation in transtensional settings: Tectonophysics, v. 457, p. 239–253.
Surpless, B.E., 2010, Geological map of the central Wassuk Range, western Nevada: Geological Society of America Map Series, MCH–98.
Surpless, B.E., Stockli, D.F., Dumitru, T.A., and Miller, E.L., 2002, Two-phase westward encroachment of Basin and Range extension into the northern Sierra Nevada: Tectonics, v. 21, no. 1, doi: 10.1029/2000TC001257.
Wernicke, B.P., 1992, Cenozoic extensional tectonics of the U.S. Cordillera, *in* Burchfiel, B.C., Lipman, P.W., and Zoback, M.L., eds., The Cordilleran Orogen: Conterminous United States, Volume G3: Decade of North American Geology: Boulder, CO, Geological Society of America, p. 553–581.
Wesnousky, S.G., 2005, Active faulting in the Walker Lane: Tectonics, v. 24, doi: 10.1029/2004TC001645.
Whitlock, J., 2002, Evidence of a mantle wedge source for slab window volcanism in the northern California Coast Ranges: Master's thesis, Pennsylvania State University, University Park, Pennsylvania, 79 p.
Whitlock, J., Furlong, K., Lesher, C., and Furman, T., 2001, The Juan de Fuca slab-window and Coast Range volcanis, California: correlation between subducted slab age and mantle wedge geochemistry: EOS Transactions, American Geophysical Union, v. 82, Abstract F1186.
Wills, S., and Buck, W.R., 1997, Stress-field rotation and rooted detachment faults: A Coulomb failure analysis: Journal of Geophysical Research, v. 102, no. B9, p. 20503–20514.
Wilson, M., 1989, Igneous petrogenesis: London, Harper Collins, 466 p.
Zoback, M.L., 1989, State of stress and modern deformation of the northern Basin and Range province: Journal of Geophysical Research, v. 94, p. 7105–7128.

Downloaded By: [Surpless, Benjamin E.] At: 14:16 19 April 2011

Appendix 1. Analytical procedures

$^{40}Ar/^{39}Ar$ age dating

Samples from the central Wassuk Range were analysed in the Stanford University $^{40}Ar/^{39}Ar$ geochronology laboratory. Mineral separates were prepared first by standard crushing and sieving techniques, then separated by techniques related to mineral gravities and magnetic susceptibilities. The separates were cleaned with distilled water in an ultrasonic bath, dried, and then hand-picked under a microscope to remove composite grains and undesired phases. Samples were packaged in Cu foil and irradiated for 16 hours at the University of Oregon TRIGA reactor using sanidine standard from the Taylor Creek Rhyolite with an assumed age of 27.92 million years (Duffield and Dalrymple 1990) as a flux monitor. Heating experiments were conducted with a double-vacuum (Staudacher-type) resistance furnace with a Ta crucible and replaceable Mo liner. Gas was extracted during heating steps with 8 minutes dwell times and 10–13 minutes of gettering using SAES Zr–Al getters. Ar isotopes were analysed over a period of 10–15 minutes using a MAP 216 mass spectrometer. Peak heights above background were measured during 7–12 serial scans of ^{40}Ar–36Ar performed for the obtained gas fraction at each temperature step. Isotopic abundances were then calculated by linear extrapolation to time zero using the computer program 'EyeSoreCon' written by B.R. Hacker (Stanford University, 1992). These data were corrected for neutron flux gradients during irradiation, decay since irradiation, and Cl-, Ca-, and K-produced Ar isotopes. Reported uncertainties are one sigma and account for uncertainties in the following: monitor age; value of irradiation parameter J; measured peak heights; dynamic blanks; and static blanks at temperature.

Trace-element geochemistry

Sample whole-rock powders were prepared using standard crushing and sieving techniques at Stanford University. Samples were then sent to the Oregon State University Radiation Center for INAA analysis.

Appendix 2. $^{40}Ar/^{39}Ar$ tabulated data for analysis of samples 96BS-50 (map unit Kqm), 95BS-62 (map unit Tlf, lower in section), 95BS-74 (map unit Tlf, higher in section), and 96BS-WR-1 (map unit Tba_1).

Sample: 96BS-50 Whole rock $J = 0.0004991$

T(°C)	40(mol)	40/39	37/39	36/39	K/Ca	$\Sigma^{39}Ar$	$^{40}Ar^*$	Age(Ma)	
600	2.10E − 14	264.6323	9.2285	0.5948	0.053	0.029	0.336	78.3	1.6
650	2.10E − 14	158.2976	2.9308	0.2798	0.17	0.078	0.478	66.8	0.7
700	2.90E − 14	139.2317	2.5271	0.1428	0.19	0.153	0.697	85.3	0.5
800	3.10E − 14	119.9852	1.0812	0.0707	0.45	0.246	0.826	87.1	0.4
850	2.40E − 14	130.0583	2.6428	0.1197	0.19	0.313	0.728	83.3	0.5
900	3.20E − 14	133.454	3.1348	0.1253	0.16	0.398	0.723	84.8	0.5
950	4.10E − 14	150.6703	7.1312	0.1618	0.069	0.497	0.683	90.3	0.5
1000	5.20E − 14	126.3196	3.5344	0.0811	0.14	0.647	0.81	89.9	0.4
1050	8.10E − 14	116.6479	1.0821	0.0404	0.45	0.898	0.898	91.9	0.5
1100	2.20E − 14	184.4795	13.7402	0.1942	0.036	0.941	0.689	110.9	0.8
1150	2.80E − 14	347.6568	25.7799	0.3775	0.019	0.972	0.679	201.0	1.6
1200	3.00E − 14	535.7001	17.5103	0.6197	0.028	0.992	0.658	292.4	4.4
1400	1.50E − 14	670.5794	13.3262	0.857	0.037	1	0.622	341.3	6.8

Steps used: 600, 700, 800, 850, 900, 950, 1000, 1050 (8 of 13 or 85% $\Sigma^{39}Ar$)

Sample: 95BS-62 Hornblende $J = 0.0005028$

T(°C)	40(mol)	40/39	37/39	36/39	K/Ca	$\Sigma^{39}Ar$	$^{40}Ar^*$	Age(Ma)	
600	2.20E − 15	108.4422	10.0374	0.3063	0.049	0.008	0.165	16.2	1.1
700	1.40E − 15	39.5333	9.6207	0.0721	0.051	0.022	0.461	16.4	0.7
800	1.30E − 15	29.8662	6.0857	0.0432	0.081	0.039	0.572	15.4	0.6
850	5.40E − 16	26.3563	5.0516	0.0328	0.097	0.047	0.632	15.1	1.1
900	3.50E − 16	28.5208	5.8096	0.0268	0.084	0.052	0.723	18.6	1.8
950	7.90E − 16	75.1554	9.3421	0.2054	0.052	0.057	0.193	13.1	2.4
1000	3.40E − 15	36.9346	6.874	0.0694	0.071	0.094	0.444	14.8	0.3
1025	3.60E − 15	30.8121	7.2887	0.0507	0.067	0.14	0.514	14.3	0.2
1050	6.20E − 15	26.9924	7.1288	0.0361	0.069	0.231	0.605	14.7	0.1
1075	1.70E − 14	25.0329	7.0252	0.0295	0.07	0.497	0.651	14.7	0.1
1100	1.60E − 14	18.3697	6.88	0.0071	0.071	0.839	0.886	14.7	0.2
1125	2.60E − 15	22.0574	9.7984	0.0171	0.05	0.887	0.771	15.4	0.2
1200	5.70 − −15	20.1974	9.9769	0.0113	0.049	1	0.835	15.2	0.1

Steps used: 1000, 1025, 1050, 1075, 1100 (7–11 of 13 or 78% $\Sigma^{39}Ar$)

Downloaded By: [Surpless, Benjamin E.] At: 14:16 19 April 2011

Sample: BS95-74 Hornblende $J = 0005041$

T(°C)	40(mol)	40/39	37/39	36/39	K/Ca	Σ^{39}Ar	^{40}Ar*	Age(Ma)	
600	7.00E − 15	113.3864	10.4804	0.3318	0.047	0.027	0.135	13.9	0.6
800	2.50E − 15	33.7668	18.2666	0.0412	0.027	0.059	0.639	19.5	0.7
860	2.50E − 15	42.5801	22.5612	0.0688	0.022	0.085	0.523	20.1	0.6
900	1.10E − 15	38.3717	21.6804	0.0447	0.023	0.097	0.656	22.7	1.2
950	1.20E − 15	50.7203	22.0231	0.076	0.022	0.108	0.557	25.5	1.4
975	7.70E − 16	44.3137	21.5107	0.0618	0.023	0.115	0.588	23.5	1.9
985	6.40E − 16	47.8938	20.031	0.0674	0.024	0.121	0.584	25.3	2.5
995	6.00E − 16	43.4552	19.9995	0.0532	0.025	0.127	0.638	25.1	2.4
1000	4.50E − 16	40.1296	13.9704	0.0312	0.035	0.132	0.77	27.9	3.0
1010	5.10E − 16	36.1055	14.0259	0.0438	0.035	0.138	0.641	20.9	2.3
1020	6.00E − 16	34.2809	11.5994	0.0382	0.042	0.146	0.671	20.8	1.9
1030	7.40E − 16	31.5298	11.5104	0.0338	0.043	0.156	0.683	19.5	1.4
1050	2.00E − 15	29.8698	10.1971	0.0375	0.048	0.185	0.629	17.0	0.5
1070	6.40E − 15	26.4684	8.0608	0.0324	0.061	0.288	0.638	15.3	0.1
1095	1.50E − 14	25.5095	8.8242	0.0298	0.056	0.545	0.655	15.1	0.1
1120	5.30E − 15	22.6044	25.1107	0.0141	0.02	0.647	0.816	16.7	0.2
1150	1.60E − 14	21.5732	14.709	0.0178	0.033	0.96	0.756	14.8	0.1
1200	1.90E − 15	21.2761	31.1095	0.0098	0.016	1	0.864	16.6	0.4

Steps used: 600, 1030, 1050, 1070, 1095, 1120, 1150, 1200 (8 of 18 or 88% Σ^{39}Ar)

Notes: Abbreviations are as follows: TFA, total fusion age; WMPA, weighted mean plateau age; MSWD, mean standard weighted deviation; atm, atmospheric ratio, of ^{40}Ar/^{36}Ar; 40(mol) = moles corrected for blank and reactor-produced ^{40}Ar; J, irradiation parameter. Column headings 40/39, 38/39, 37/39, and 36/39 refer to Ar isotopic ratios; the Σ^{39}Ar column is the cumulative amount of ^{39}Ar released; and ^{40}Ar* is the percentage of radiogenic ^{40}Ar. Steps used refer to those temperature steps used to calculate the plateau and isochron ages. Ages given for steps are 1σ. Dwell time for each temperature step was 8 min. Ratios are corrected for blanks, decay, and interference.

Downloaded By: [Surpless, Benjamin E.] At: 14:16 19 April 2011

Downloaded By: [Surpless, Benjamin E.] At: 14:16 19 April 2011

Appendix 3. Whole-rock trace-element analyses for Mesozoic and Cenozoic rocks.

Unit sample	Tertiary basaltic andesites (Tba)									Late-stage dikes		
ppm	95-26	95-33	96-73	97-12	97-39	97-41	97-42	97-67	97-70	97-7	96-32	97-75
Se	15.90	11.90	18.10	13.90	11.90	13.90	9.63	15.10	15.40	38.60	24.70	26.40
Cr	23	4	108	91	110	69	106	218	56	49	< 14	332
Co	23.90	17.00	20.90	20.00	17.70	20.00	11.70	28.30	18.10	32.60	13.50	18.10
Ni	< 140	< 93	71	76	96	90	81	142	99	< 200	< 140	127
Zn	80	89	90	92	71	84	52	74	79	162	110	42
As	3.4	6.4	11.1	16.3	9.5	6.8	30.0	8.5	4.5	2.0	< 6.0	3.0
Sb	0.48	0.33	1.18	2.92	1.55	1.46	0.90	1.30	0.78	2.53	0.73	1.80
Se	< 4.2	< 2.6	< 4.2	1.0	0.5	0.8	< 0.81	< 1.1	< 1.1	< 4.8	< 3.6	1.1
Rb	50	51	82	113	41	85	61	60	60	325	11	16
Cs	1.20	1.00	2.70	6.85	2.17	2.18	1.43	2.47	1.65	11.60	0.44	0.63
Sr	739	874	790	799	1030	989	953	977	1170	452	405	654
Ba	1260	1130	1060	1080	1210	1230	1930	1170	1470	539	195	398
La	30.7	24.9	39.6	51.3	23.6	40.4	27.0	22.6	33.2	11.9	28.1	16.6
Ce	56.3	48.4	75.6	101.0	49.3	80.2	58.4	53.3	69.8	270	63.5	32.3
Nd	27.6	27.0	36.2	45.8	22.3	36.1	35.1	21.6	36.5	17.8	33.2	18.3
Sm	5.45	5.07	7.44	8.56	4.31	7.26	5.96	4.51	6.17	3.26	7.33	3.96
Eu	1.42	1.42	1.54	1.58	1.05	1.57	1.23	1.13	1.56	1.05	1.89	1.69
Tb	0.62	0.60	0.77	1.00	0.50	0.79	0.44	0.53	0.66	0.45	0.94	0.51
Yb	1.6	2.0	2.5	2.5	1.4	2.1	0.9	1.4	1.8	1.7	3.2	1.6
Lu	0.22	0.27	0.33	0.38	0.18	0.26	0.14	0.17	0.23	0.24	0.46	0.22
Zr	94	80	150	148	70	136	85	106	74	< 190	133	90
Hf	3.16	3.67	7.16	9.36	4.17	7.50	3.68	4.15	3.81	1.19	3.99	2.07
Ta	0.36	0.44	0.55	0.79	0.32	0.63	0.35	0.27	0.36	0.15	0.46	0.25
W	1.7	< 3.6	2.9	2.4	1.4	3.5	< 2.7	1.5	1.3	< 5.7	2.2	< 4.8
Hg	< 0.084	< 0.063	< 0.078	< 0.048	0.04	< 0.045	0.02	< 0.060	< 0.057	< 0.10	< 0.090	< 0.066
Th	5.8	4.5	12.7	16.5	5.4	13.6	8.2	5.4	7.7	1.8	7.4	2.0
U	1.8	1.7	4.6	6.3	2.4	4.6	3.2	2.0	3.0	< 4.8	2.2	3.7

(*Continued*)

Downloaded By: [Surpless, Benjamin E.] At: 14:16 19 April 2011

Appendix 3. (*Continued*).

Unit sample	Tertiary hornbiende andesites (Tlf)						Tsi*	Tmp*	OIB**	Kgm	Jhqm
ppm	96-70	96-72	97-16	97-29	97-30	97-46	95-89	95-90		96-44	97-22
Sc	8.47	5.67	13.30	12.10	7.13	10.70	9.12	2.77		7.71	5.03
Cr	17	13	79	37	23	41	38	5		4	28
Co	11.30	6.98	18.20	16.00	9.71	13.80	11.30	1.06		5.33	2.32
Ni	< 99	< 110	133	67	33	54	35	< 39		< 96	39
Zn	66	61	74	78	67	65	59	33		43	15
As	3.0	3.9	3.7	5.9	5.8	2.9	4.4	4.1		< 5.4	5.0
Sb	1.86	0.41	0.93	0.70	0.46	0.50	092	0.88		0.36	1.33
Se	< 3.3	< 2.2	< 0.96	< 0.84	0.7	0.6	1.0	2.0		< 3.9	1.2
Rb	61	66	42	48	61	56	109	173	22	73	140
Cs	2.44	2.11	1.16	1.66	1.12	1.20	2.99	4.43		2.43	2.00
Sr	805	745	911	1210	1010	880	354	79	800	328	510
Ba	1090	1190	1130	1720	1230	1130	912	323	380	1120	1120
La	23.8	25.1	19.5	37.7	34.6	20.8	30.9	39.4	35	21.5	16.1
Ce	46.2	48.7	37.6	73.7	59.6	38.9	54.6	66.1	72	36.4	38.5
Nd	21.7	22.3	17.8	35.8	27.7	20.7	23.0	25.9	35	13.9	14.3
Sm	3.95	3.76	3.89	6.85	5.08	3.99	4.36	4.33	13	2.77	3.36
Eu	1.02	0.95	1.09	1.71	1.17	1.05	0.96	0.46		0.81	0.68
Tb	0.46	0.46	0.46	0.75	0.49	0.44	0.51	0.26		0.40	0.59
Yb	1.6	1.4	1.2	1.8	1.6	1.2	1.6	1.8		1.4	1.9
Lu	0.20	0.22	0.18	0.26	0.21	0.15	0.23	0.31		0.24	0.28
Zr	88	75	67	77	71	70	102	61	220	47	79
Hf	3.78	3.99	3.06	3.93	4.24	3.14	4.30	3.75		2.49	4.74
Ta	0.35	0.42	0.32	0.31	0.45	0.33	0.56	1.08	3	0.25	0.69
W	< 5.1	< 2.8	1.5	2.2	< 2.2	2.0	< 3.9	1.2		< 6.0	< 1.3
Hg	< 0.072	< 0.057	< 0.048	0.04	< 0.042	0.01	< 0.063	< 0.033		< 0.063	< 0.039
Th	52	6.0	3.8	8.0	7.8	4.7	11.9	21.2	3	7.3	27.0
U	1.5	2.0	1.8	3.1	2.9	1.5	2.5	4.5	1	2.1	6.1

Notes: INAA analyses were performed at Oregon State University of Corvallis, Oregon, as a part of the DOE's Reactor Sharing Programme. Values are expressed in ppm.
*Tsi = Singatse tuff; Tmp = Mickey Pass tuff (both part of map unit Ttu)
**Representative values from Sun (1980)